



Review

Molecular modelling for transition metal complexes: Dealing with d-electron effects

Robert J. Deeth*, Anna Anastasi, Christian Diedrich, Kris Randell

Inorganic Computational Chemistry Group, Department of Chemistry, University of Warwick, Coventry CV4 7AL, UK

Contents

1. Introduction	796
1.1. Computational methods and implicit electronic effects	796
1.2. Explicit electronic effects	797
2. Molecular mechanics and ligand field theory	798
2.1. The angular overlap model	798
2.2. Molecular mechanics and molecular dynamics	800
2.2.1. Shortcomings of MM for TM systems	801
2.3. Ligand field molecular mechanics	802
3. Applications of LFMM	803
3.1. Simple coordination complexes: Cu(II) amines	803
3.2. $[\text{MCl}_4]^{2-}$ complexes	803
3.3. Cu(II) bis-oxazoline complexes	804
3.4. Siderophore complexes: systems with zero LFSE	805
3.5. Jahn–Teller effects in six-coordinate Cu(II) complexes	805
3.5.1. The Mexican hat potential energy surface	806
3.5.2. The warped Mexican hat	806
3.5.3. Theoretical treatment of the Jahn–Teller effect in Cu(II) species	807
3.5.4. Barriers between successive elongations	807
3.5.5. Truly compressed complexes	808
3.5.6. Cu(II) Jahn–Teller effects: summary	809
3.6. Spin-state effects	810
3.7. Type 1 copper enzymes	811
3.8. Dinuclear copper centres	813
4. Other approaches	814
4.1. SIBFA-LF	814
4.2. GULP	814
4.3. Effective crystal field and deductive molecular mechanics	815
5. Conclusions	815
References	815

ARTICLE INFO

Article history:

Received 5 April 2008

Accepted 28 June 2008

Available online 9 July 2008

Keywords:

Ligand field theory

Molecular mechanics

Jahn–Teller

Spin states

Copper enzymes

ABSTRACT

The development and application of molecular mechanics methods which include an explicit treatment of d-electron effects are reviewed. The origins of the authors' ligand field molecular mechanics (LFMM) method are traced from Hitchman's simple expression for predicting the M–L bond length change accompanying a d–d transition through to the general implementation of LFMM within the molecular operating environment, including analytical energy gradients, explicit M–L π -bonding and d–s mixing effects, plus a term for handling different spin states. The LFMM applications cover simple coordination complexes of Cu(II) where a single parameter set treats multiple coordination numbers; the treatment of the complete Jahn–Teller effect in six-coordinate d^9 Cu(II) complexes including elongated and compressed structures and the intervening barrier height; the parameterisation of Co(III) and Ni(II) species to enable both high- and low-spin complexes to be treated with a single parameter set; the unusual and highly distorted Type 1

* Corresponding author. Tel.: +44 2476 523187.

E-mail address: r.j.deeth@warwick.ac.uk (R.J. Deeth).

centre in 'blue copper' enzymes; and dinuclear species containing the $[\text{Cu}_2\text{O}_2]^{2+}$ moiety found in Type 3 copper enzymes and the important Cu–O π -bonding effects. The LFMM has also spawned two approaches, the ligand field extension of the sum of interactions between fragments *ab initio* (SIBFA) model and an extension to the general utility lattice program (GULP). The former has been applied to some simple Cu(II) species while the latter has been applied to d^4 Mn(III)-oxides. Both are limited to σ effects only. In addition, the related effective crystal field model of Tschougreeff is discussed and compared with the LFMM approach. Providing one is prepared to develop the necessary parameters, the LFMM and related approaches are capable of delivering DFT-quality results but up to four orders of magnitude faster.

© 2008 Elsevier B.V. All rights reserved.

1. Introduction

The structures and reactivity of classical Werner-type coordination complexes are profoundly influenced by the d electrons. A classic example is the 'double-hump' variation of thermodynamic and structural properties, particularly of first-row metal complexes. For example, the experimental hydration enthalpies of the divalent aqua ions (black diamonds, Fig. 1) deviate substantially from any monotonic variation on crossing the series from left to right [1].

Perhaps the simplest model for describing d orbital energies is ligand field theory (LFT) [2] which was itself derived from the earlier electrostatic crystal field theory (CFT) [3] approach. In LFT, we focus on a limited number of states which can be derived from the terms arising from the d^n configuration. These comprise the ground state and those excited states which we associate with d–d electronic excitations and their relative energies are expressed parametrically. The properties which can be computed by LFT are thus limited. Nevertheless, with a careful formulation [3], LFT and its attendant parameters provide a useful, semi-quantitative picture of metal–ligand coordination in Werner complexes which has been successfully exploited for over half a century [4–6]. LFT also generates a simple rationalisation of the double-hump behaviour depicted in Fig. 1 in terms of the ligand field stabilisation energy (LFSE).

The LFSE is a function of the d configuration and the magnitude of the ligand field splitting. The latter can be independently derived from spectroscopic data by fitting the d–d absorption bands of these nominally octahedral species [7]. The LFSE is often considered to be a simple function of Δ_{oct} (Fig. 2) and if the experimental hydration enthalpies are 'corrected' using the spectroscopic Δ_{oct} values, a remarkably smooth line is obtained (open circles in Fig. 1).

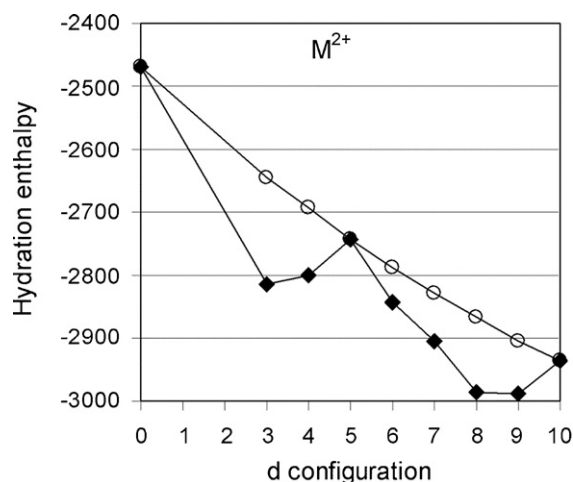


Fig. 1. Variation of experimental hydration enthalpies (solid diamonds) from d^0 Ca^{2+} through to d^{10} Zn^{2+} . The open circles represent the values once d electron stabilisation energy effects are removed (after Johnson and Nelson [1]).

However, while this simple picture works well for divalent metals, the LFSE itself is more complicated and may include contributions in addition to the d electron term depicted in Fig. 2. For example, in trivalent aqua complexes, d–d interelectronic effects become relatively more important [8]. Nevertheless, if we interpret the LFSE in its broadest sense and include both one-electron (Δ_{oct} or spectrochemical) and two-electron (interelectronic repulsion and thereby nephelauxetic) contributions, the conclusion is that the LFSE makes a substantial contribution to the properties of coordination complexes. Therefore, computational methods for modelling them must account for the LFSE. However, this can be achieved implicitly or explicitly.

1.1. Computational methods and implicit electronic effects

By construction, electronic effects are implicit in quantum mechanical (QM) methods. However, QM treatments of Werner-type transition metal (TM) systems present many challenges. In contrast to most organic and organometallic species, they are frequently paramagnetic with complicated electronic ground states and many, low-lying excited states. Additionally, they often carry a net charge and so environmental effects, notably solvation, can be significant [9].

Very significant progress has been achieved especially over the last two decades where a revolution in quantum chemistry for TM species has occurred in the form of density functional theory (DFT). Compared to wavefunction methods like Hartree–Fock theory and its correlated extensions, DFT is relatively quick and accurate and has established an impressive reputation for TM species [10]. Especially in its hybrid B3LYP form, DFT has become the *de facto* standard for quantum chemical modelling of coordination complexes including those of biological relevance [11]. Of course, no current functional is perfect, including B3LYP, and the quest for better functionals continues [12]. However, while we can argue the merits of different pure and hybrid functionals, all quantum methods are relatively compute intensive which ultimately limits the size of system and/or the type of calculation which can be achieved in a reasonable time.

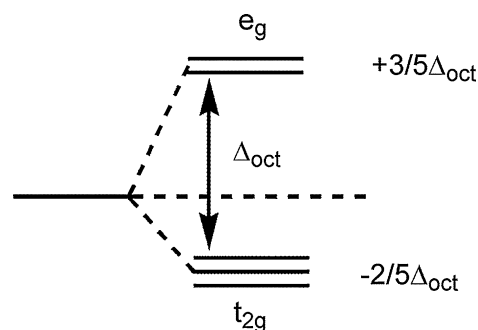


Fig. 2. Octahedral d-orbital splitting diagram from which the one-electron contribution to the LFSE can be computed.

An alternative to fully quantum approaches is semi-empirical MO theory which combines a minimal basis quantum treatment of the valence orbitals with a simplified and parametric treatment of core effects. Such methods are very much faster than full QM but their application to TM systems has been restricted partly since only selected metals are parameterised and partly since the accuracy is patchy, especially with respect to open d shell systems. Nevertheless, the improved computational efficiency is attractive and many successful applications of semi-empirical methods have been reported such as a study of the structural and electronic properties of Fe(III) complexes with N/S donors relevant to nitrile hydratase [13] and the *de novo* prediction of structure and spin states for a range of Tc complexes using a modified version of PM3(tm) [14]. New parameterisations such as PM6 [15] and AM1* [16] promise improved accuracy over previous semi-empirical schemes and a much wider coverage of d electron systems but the absolute errors in heats of formation and geometrical data are, for most TMs, still quite large. Of course, for many practical applications, only the relative error is significant and these are always likely to be much less due to error cancellations. However, these methods are too recent for this aspect to have been fully explored. Meanwhile, another option is to dispense with quantum schemes and develop a classical model such as molecular mechanics (MM).

MM has the advantage of very rapid execution times, even compared to semi-empirical MO theory, but its application to TM species is complicated [17]. In conventional MM, the all-important electronic effects are again incorporated implicitly. Hence, just as the electronic consequences of sp^3 , sp^2 and sp hybridisation at carbon centres are implicitly accounted for *geometrically* by defining separate parameters sets for tetrahedral, trigonal and linear bonding respectively, so too can the electronic effect of, say, a low-spin d^8 configuration be accommodated by applying an out-of-plane function to the metal centre which then forces it to remain planar, or the Jahn–Teller distortion in CuL_6 species can be treated by defining different parameters for short equatorial and long axial bonds even though the ligands may be chemically identical [18].

These two examples serve to illustrate that the application of conventional MM to TM systems may lead to loss of generality. For example, the vast majority of four-coordinate $Ni(II)N_4$ complexes are planar low-spin. However, if the steric requirements of the ligand prevent planar coordination, the high-spin, tetrahedral state is favoured (1, Fig. 3). However, in conventional MM, there are different parameter sets for high-spin and low-spin systems [19] and the user must decide *a priori* which one to use plus, given different FFs have different reference states, the potential energies of high-spin and low-spin forms cannot be directly compared and hence conventional MM cannot be used to predict which spin state is the lowest. In contrast, since QM explicitly treats electrons, the high-spin and low-spin forms correspond to simple rearrangements of the electrons. Hence, the reference states are the same and, in principle at least, the total energies can be compared directly. Of course, the *accuracy* of such a comparison is an open question. Reliable prediction of relative spin-state energies is a well known problem for QM approaches in general and DFT in particular [20–23].

The second example of Jahn–Teller distortions in $Cu(II)L_6$ systems also highlights the shortcomings of conventional MM. In principle, for a simple complex like $[Cu(NH_3)_6]^{2+}$, there are three equivalent elongation axes. In this case, the choice is irrelevant but this may not apply for mixed-ligand systems. Consider, for example, CuA_4B_2 systems where A and B represent different donors. The temptation might be to assume that the elongation axis would correspond to the ‘minority’ ligand B which is in agreement with experimental X-ray crystal structure data for complex 2 in Fig. 4 but not for complex 3. Moreover, although tetragonal elongations are usually observed, some ligands force a tetragonal compression (4).

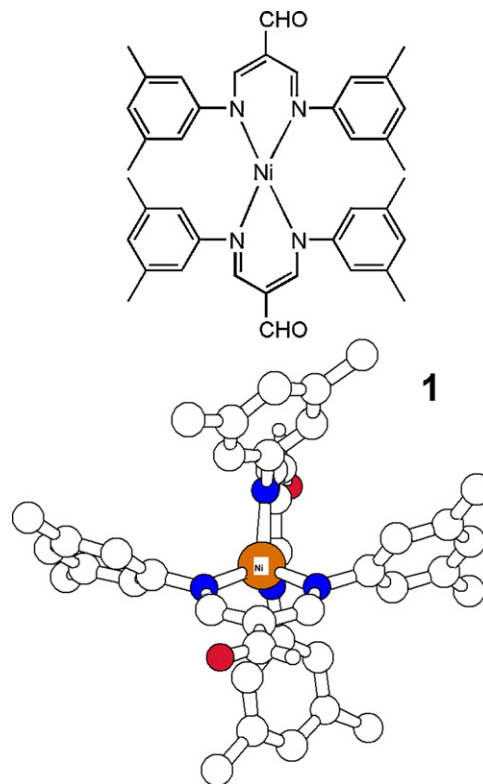


Fig. 3. Tetrahedral, high-spin d^8 NiN_4 complex bis(bis(*N*-(3,5-dimethylphenyl)imino)-2-formyl-1-propenyl)-3,5-dimethylanilinato-*N,N'*-nickel(II). The non-planar structure is enforced by the ligand. Non-polar hydrogens omitted for clarity.

In the latter example, the tertiary butyl substituents on the imine nitrogens are critical and smaller groups lead to an elongated structure where the long bonds are to the pyridyl donors [24,25]. Such a swap in elongation axis cannot be captured automatically by a conventional MM treatment.

Despite these apparent shortcomings, conventional MM can be, and has been, applied to coordination complexes on numerous occasions for a variety of properties [18]. However, the subject of this review is directed towards the extension of MM to include explicitly the important electronic effects which QM methods treat implicitly. Thus, we generate an empirical approach which combines the flexibility and generality of QM with the speed of MM.

1.2. Explicit electronic effects

Explicit treatment of electronic effects within MM, which is the main subject of this review, requires some extension of the basic MM formalism. In particular, new potential energy terms to describe the effects of the LFSE need to be included [17]. Since the simplest model for d electron effects is ligand field theory, we suggested in 1995 a marriage between LFT and MM in order to capture the essential physics of d electron stabilisation in a fast empirical method [26,27]. Our inspiration for this and the subsequent development of LFMM arose from Hitchman's simple model for predicting the M–L bond length changes, δr , accompanying certain d–d excitations [28]. If the transition corresponds to depopulating an M–L π -type orbital and placing the electron(s) in the σ^* -type M–L orbital, a significant change in M–L bond length results which has a substantial LFSE component.

Hitchman's equation (1) relates to M–L bond length change to the number of electrons involved in the change, m , the energy sep-

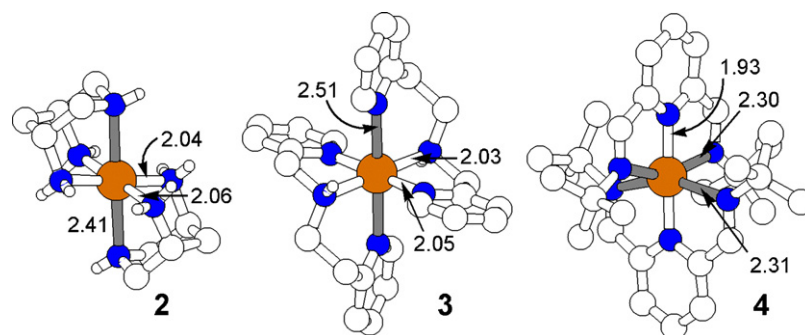


Fig. 4. Jahn–Teller distorted Cu(II) complexes. (Non-polar H atoms omitted for clarity.).

aration of the orbital involved in the change, Δ , the initial bond length, r_0 , the force constant for the symmetric stretch vibration, f , and the number of ligands coordinated to the metal, N . The final parameter, n , relates to the assumption that Δ depends inversely on some power, n , of the bond distance. In simple crystal field theory, for example, $n = 5$.

$$\delta r \simeq \frac{nm\Delta}{fr_0N} \quad (1)$$

Hence, the structural change is interpreted as a simple balance between electronic and vibrational contributions. This idea was later successfully extended by Hitchman and one of the present authors (RJD) to the more complicated situation of predicting the magnitude of the Jahn–Teller distortions in systems with formally doubly-orbitally-degenerate E ground states [29]. The electronic energies were estimated on the basis of the angular overlap model (AOM) [30] which describes the total ligand field potential as a sum of individual, local M–L contributions rather than in terms of the global symmetry as had been introduced originally in crystal field theory and then carried over into LFT [2]. This ‘bond-centered’ AOM is ideally suited to MM as described in the next section.

The link between electronic and geometrical structure inherent in the AOM was also exploited to estimate the structures of $[\text{CuCl}_4]^{2-}$ complexes doped to about 0.1 mol% into crystals of diamagnetic $[\text{ZnCl}_4]^{2-}$ species [31]. Assuming a C_{2v} geometry and ‘reasonable’ values for the AOM Cu–Cl σ and π bonding parameters (*vide infra*), the d–d transition energies and EPR g -values were expressed as a function of the angles α and β illustrated in Fig. 5.

By fitting the experimental data to the theoretical expressions, estimates of α and β were obtained which were consistent with the doped copper species adopting an intermediate geometry with features of the host zinc structure superimposed on the intrinsic ‘flattened’ tetrahedral structure of $[\text{CuCl}_4]^{2-}$ where $\alpha = \beta \sim 128^\circ$. Most $[\text{ZnCl}_4]^{2-}$ complexes such as that in Cs_2ZnCl_4 are essentially tetrahedral but $(\text{enH}_2)_2\text{ZnCl}_4 \cdot 2\text{Cl}$ is exceptional with $\alpha = 125^\circ$ –

significantly larger than the tetrahedral value – and $\beta = 107^\circ$, somewhat smaller than the tetrahedral value. The spectroscopic data for the doped copper species were similarly unusual, especially the EPR spectra which displayed very rhombic g -values (2.0077, 2.1203, 2.4356 compared to the ‘normal’ $[\text{CuCl}_4]^{2-}$ species in $\text{Cs}_2\text{Zn}[\text{Cu}]\text{Cl}_4$ with g -values of 2.078, 2.080, 2.437) and an unusually small copper hyperfine splitting along the z -axis, a feature mimicked in the highly distorted active site of ‘blue’ copper proteins (see 3.7). The best-fit angles of the doped complex in $(\text{enH}_2)_2\text{ZnCl}_4 \cdot 2\text{Cl}$ were predicted to be 135.5 and 113.0° compared to those in Cs_2ZnCl_4 of 126.7 and 123.2° .

2. Molecular mechanics and ligand field theory

As mentioned in Section 1.2, this review focuses on the inclusion of an explicit treatment of d-electron effects within molecular mechanics. These effects can be conveniently handled via ligand field theory with the bond-centered AOM being especially suited.

2.1. The angular overlap model

The AOM came to prominence in the mid-1960s largely through the work of Schaeffer and Jorgensen [30]. It embodied the principle of ligand superposition in that it was assumed that the total ligand field potential, V_{LF} , could be constructed as a sum of contributions from individual M–L bonds and that these contributions were essentially localised. Hence, the local ligand field perturbation could be described in terms of local bonding interactions. In particular, the complex could effectively be treated as a set of diatomic molecules with the bonds divided into separate σ and π contributions which were modelled by AOM parameters such as e_σ , $e_{\pi x}$ and $e_{\pi y}$ as illustrated in Fig. 6.

A critical feature of the AOM, and the source of its original popularity, was that this construction could make contact with local chemical bonding concepts, a feature singularly lacking from the global crystal field theory approach prevalent at that time. The AOM makes a clean separation between the angular contributions to V_{LF} , which are inherent in the molecular structure and therefore ‘automatically’ accounted for, and the radial contributions which relate to the nature of the metal–ligand bonding and are embodied in the e parameters.

In principle, each d-orbital energy becomes a function of the AOM parameters of all the ligands. The contribution to a given d function from a particular ligand can be couched in terms of the square of the orbital overlap, S^2 , between the d function and a suitable ligand-based orbital. For example, the construction on the left of Fig. 6 shows that when the ligand is oriented directly at the large lobe of d_{z^2} ($S^2 = 1$) the full ‘ e_σ ’ worth of destabilisation is transferred. However, for a ligand in an equatorial position, the ratio of the overlap between the large lobe and the equatorial ‘belly band’ of the d_{z^2}

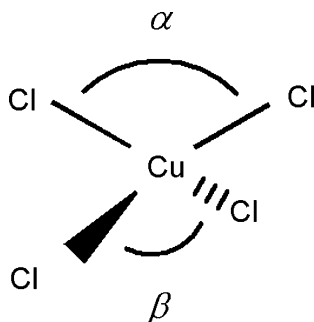


Fig. 5. Definition of α and β in C_{2v} symmetric $[\text{CuCl}_4]^{2-}$ complexes.

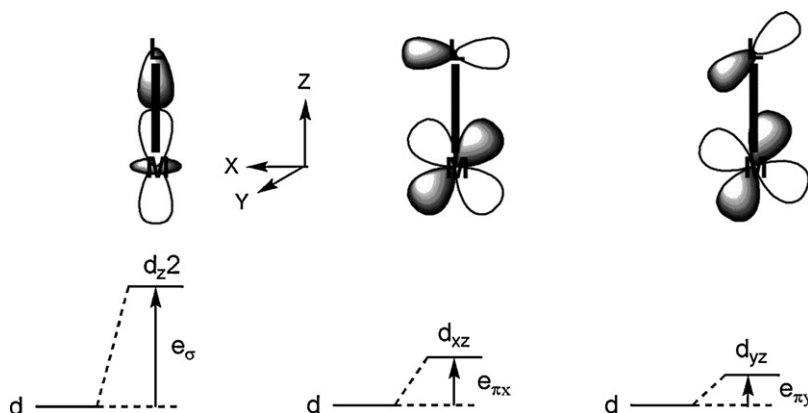


Fig. 6. Definition of AOM e parameters in terms of local M–L bonding. The σ interaction is always destabilising ($e_\sigma > 0$) while π -bonding in the two mutually perpendicular directions to the M–L vector (the local z -axis) is shown for a π donor ($e_\pi > 0$).

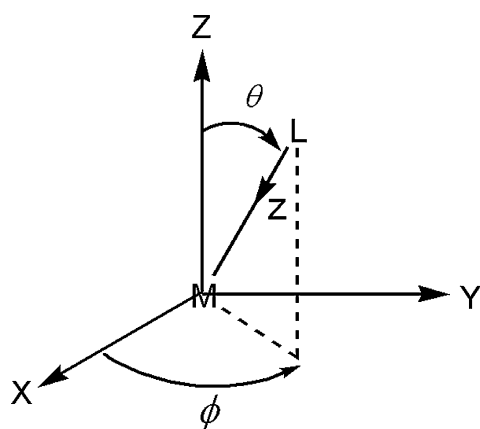


Fig. 7. Definition of angular coordinates θ and ϕ for a ligand L relative to the global Cartesian axis frame. The lower case z refers to the local M–L axis frame.

function is 4:1, i.e. $S^2 = 0.25$ and an equatorial ligand destabilises d_{z^2} by $(1/4) e_\sigma$.

The precise relationship between a given AOM parameter for a given ligand and its effect on a given d orbital is given by the so-called F factor which is a trigonometric function of the ligand's angular coordinates, θ and ϕ (Fig. 7).

For the particular case of a σ interaction with the d_{z^2} orbital, since the orbital is cylindrically symmetry about the global Z axis, its energy, $E(d_{z^2})$, depends only of the θ coordinate as given in Eq.

(2). The complete form of F_θ^2 is displayed in Fig. 8.

$$E(d_{z^2}) = F_\theta^2(d_{z^2})e_\sigma = \frac{1}{16}(1 + 3 \cos 2\theta)^2 e_\sigma \quad (2)$$

As the ligand moves relative to the d orbitals, it may interact with other d functions. In the example above, as the ligand moves onto the x -axis, it interacts directly with $d_{x^2-y^2}$ and since the ratio of the sizes of the large d_{z^2} lobe and a lobe of $d_{x^2-y^2}$ is 4:3 (equivalently, the ratio of the relevant F^2 factors is 4:3) the ligand destabilises the latter orbital by $3/4 e_\sigma$. Thus, the full amount of M–L σ bonding is, in this simple case, distributed over two orbitals.

In a more general sense, the elements from which $5 \times 5 V_{LF}$ matrix is constructed are expressed in terms of angular factors, F , which depend on the coordinates of the N ligands, and the AOM radial e_k parameters, where $k = \sigma, \pi_x$ and π_y (3). Since V_{LF} is Hermitian there is a maximum of 15 unique elements but since LFT only computes energy differences relative to the ground state, a theoretical maximum of 14 degrees of freedom can be employed to fit experimental data. Moreover, as the symmetry becomes lower, the off-diagonal elements of V_{LF} will be non-zero so that the matrix will have to be diagonalised to extract the actual d orbital energies.

$$\langle d_i | V_{LF} | d_j \rangle = \sum_l \sum_k^{\text{symm}} F_{ik}^l F_{kj}^l e_k^l \quad (3)$$

Early applications of the AOM established correlations between the magnitudes and signs of the AOM e parameters and the nature of the metal–ligand bonds [7]. In principle, each ligand could be assigned its own unique set of parameters but this soon leads to an intractable fitting procedure with more parameters than can be supported by the experimental data. The classic example is octahedral O_h symmetry which, as group theory dictates, has only one degree of freedom with respect to the d orbital splitting but which generates 18 AOM parameters from six ligands. However, a practical and chemically sensible assumption of ‘chemical equivalence’ – i.e. using the same parameter values for more than one ligand – drastically reduces the number of parameters. In the O_h example where group theory imposes a rigorous chemical equivalence, a single e_σ value suffices for all six ligands while the four-fold symmetry around each M–L bond ensures that the local x - and y -axes (the local z -axis is always assumed to lie along the M–L vector) are equivalent and hence $e_{\pi_x} = e_{\pi_y}$ and only two AOM parameters are required.

In AOM terms, the octahedral splitting Δ_{oct} is given by (4) and illustrated in Fig. 9 for the particular case of a π -donor ligand for

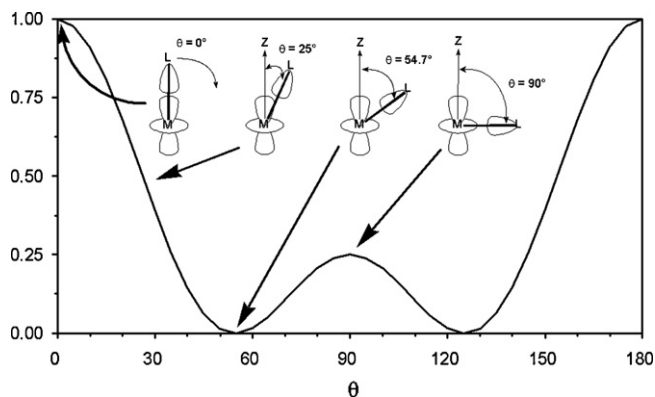


Fig. 8. Effect of angular variation on proportion of e_σ affecting the energy of the d_{z^2} orbital.

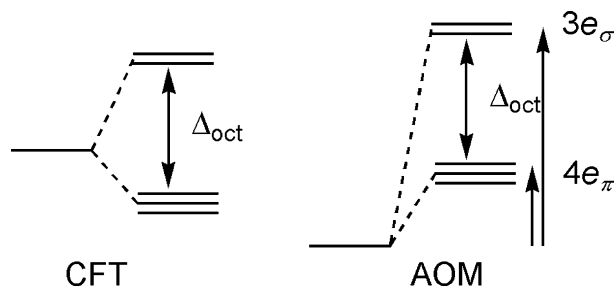


Fig. 9. Comparison of CFT barycentre (left) versus AOM barycentre (right).

which e_{π} is positive.

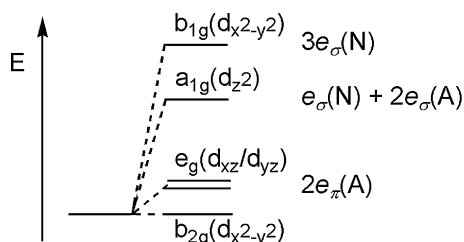
$$\Delta_{\text{oct}} = 3e_{\sigma} - 4e_{\pi} \quad (4)$$

The problem is still underdetermined. However, if it can be assumed that one parameter is zero – e.g. $e_{\pi} = 0$ for amine ligands – or if a parameter value for a given complex can be assigned a value based on the analysis of another for which a good fit is possible – i.e. if the parameters are transferable – then unique fits are possible. Alternatively, and this is where the real strength of the AOM emerges, we can consider lower symmetry complexes where there is inherently more information in the experimental data.

For example, consider the AOM treatment for tetragonal D_{4h} systems of general formula MN_4A_2 , where the N donors are chemically equivalent σ -only amine ligand and A are so-called cylindrically symmetric donor like a halide (hence $e_{\pi x} \equiv e_{\pi y} = e_{\pi}$) (Fig. 10) [32]. Within this point group, the d orbitals transform into four sets – a_{1g} , b_{1g} , b_{2g} and e_g corresponding to d_{z^2} , $d_{x^2-y^2}$, d_{xy} , and d_{xz}/d_{yz} respectively. There are exactly three degrees of freedom inherent in the splitting pattern but since exactly three AOM parameters are required, a unique fit is possible providing the precise order of the d functions is known.

The ‘global symmetry’ CFT scheme also has three parameters, Dq, Ds and Dt, where Dq describes the cubic component of the potential, V_{oct} , upon which a tetragonal perturbation, V_{tetrag} , is imposed [33]. This construction results in the tetragonal crystal field parameters Ds and Dt depending, respectively, on the Y_2^0 and Y_4^0 spherical harmonics such that “the crystal field effect of the four equatorial ligands in a tetragonally distorted molecule is regarded as representative of an octahedral field, V_{Oh} upon which V_{tetrag} is a perturbation” [33].

While this is fine from a symmetry perspective, it does not account for the possible interplay between axial and equatorial donors. Thus, if the axial coordination affects the equatorial ligands, the latter might no longer be ‘representative’ of the nominal octahedral MN_6 system. The problem is seen when comparing the



D_{4h} MN_4A_2 : N σ only, $e_{\sigma}(N) > e_{\sigma}(A)$; $e_{\pi}(A) > 0$

Fig. 10. AOM d-orbital energy level diagram for tetragonal MN_4A_2 system.

global approach with the AOM approach for tetragonal Ni(II) systems comprising an equatorial N_4 -donor macrocycle with two axial halide or pseudo halide ligands [32].

Since both CFT and the AOM require three parameters, there is a straightforward relationship between the two theories (5)–(7) [32]. It is trivial to ‘translate’ the reported values of Dq, Ds and Dt into equivalent set of AOM parameters.

$$e_{\sigma}(N) = \left(\frac{10}{3}\right) Dq \quad (5)$$

$$e_{\sigma}(A) = \left(\frac{10}{3}\right) Dq - 2Ds - \left(\frac{5}{2}\right) Dt \quad (6)$$

$$e_{\pi}(A) = -\left(\frac{3}{2}\right) Ds + \left(\frac{10}{4}\right) Dt \quad (7)$$

However, for several complexes, this exercise generated negative e_{π} values for axial chlorides. That is, the CFT analysis was thus actually suggesting Cl^- acting as a π acceptor. The justification of the CFT study was that the parameters appeared ‘reasonable’. They were based on an analysis of unassigned d–d spectra. We suggested an equally valid but different assignment of the absorption maxima which removed the chemical inconsistency of chloride π acceptors.

The conclusion from this and many other analyses is that the AOM in its own right provides a viable basis for describing the electronic structures and bonding in coordination complexes. Moreover, since it is bond-centered, merging the AOM into molecular mechanics is conceptually simple. But before describing this, a brief résumé of MM is presented.

2.2. Molecular mechanics and molecular dynamics

Molecular mechanics treats the system as a collection of atoms connected by (possibly anharmonic) ‘springs’. Electrons are not considered explicitly (although electrostatic interactions can be included by assigning to each atom a partial atomic charge) and, in its simplest form (8), the total potential energy, E_{tot} , is expressed as a simple sum of terms describing respectively bond stretching, E_{str} , angle bending, E_{bend} , torsional twisting, E_{tor} , and non-bonding interactions, E_{nb} . The latter can include both van der Waals (vdW) and electrostatic terms.

$$E_{\text{tot}} = \sum E_{\text{str}} + \sum E_{\text{bend}} + \sum E_{\text{tor}} + \sum E_{\text{nb}} \quad (8)$$

Each term in (8) is represented by a relatively simple mathematical expression. For example, the harmonic oscillator approximation is often used for E_{str} (9) where for each unique type of bond in the system with an actual length of r we need to define the reference bond length, r_0 , and the associated force constant, k_{str} , which describes the energy penalty for deviations of the actual bond length from its ‘target’ reference value.

$$E_{\text{str}} = k_{\text{str}}(r - r_0)^2 \quad (9)$$

Other simple expressions can be defined for the remaining terms in (8) such as those given in (10) where the k are appropriate force constants, θ are bond angles, τ are torsion angles, n is the torsional periodicity parameter, ϕ the torsion offset, ρ are partial atomic charge, ε is the dielectric constant, A and B are Lennard–Jones vdW parameters and the summations run over bonded atom pairs (ij), angle triples (ijk) and torsional quadruples ($ijkl$). The non-bonded terms are summed over the distances, d_{ij} , between unique atom pairs excluding bonded pairs and the atoms at either end of an angle triple. For the atoms at the ends of a torsion quadruple, the

non-bonded term may be omitted or scaled.

$$E_{\text{tot}} = \sum_{i,j} k_{ij}(r_{ij} - r_{0,ij})^2 + \sum_{i,j,k} k_{ijk}(\theta_{ijk} - \theta_{0,ijk})^2 + \sum_{i,j,k,l} k_{ijkl}[1 + \cos(n_{ijkl}\tau - \phi_{ijkl})] + \left[\sum_{i < j} \frac{\rho_i \rho_j}{\varepsilon d_{ij}} + \sum_{i < j} \left(\frac{A_{ij}}{d_{ij}^{12}} - \frac{B_{ij}}{d_{ij}^6} \right) \right] \quad (10)$$

These potential energy terms and their attendant empirical parameters together define the force field (FF). More complicated FFs which use different and/or more complex functional forms are also possible. For example, the simple harmonic oscillator expression for bond stretching can be replaced by a Morse function, E_{Morse} (11) or additional FF terms may be added such as the stretch-bend cross-terms, E_{stb} (12), used in the Merck molecular force field (MMFF) [34–37] which may be useful for better describing vibrations and conformational energies.

$$E_{\text{Morse}} = D\{1 - e^{a(r-r_0)}\}^2 - D \quad (11)$$

$$E_{\text{stb}} = \sum_{i,j,k} \{k_{ijk}(r_{ij} - r_{0,ij}) + k_{kji}(r_{jk} - r_{0,jk})\}\theta_{0,ijk} \quad (12)$$

MM is a very successful model but it is clear from expressions such as (10) that the FF may comprise a very large number of parameters and since the quality of the FF will depend crucially on these parameters, developing a truly ‘universal’ FF is an enormous (perhaps impossible) challenge [38]. Consequently, most FFs were originally designed for a specific class of molecular system such as small organic molecules (e.g. MMFF [34–37]), or large biomolecules like proteins and DNA (e.g. AMBER [39] or CHARMM [40]). Fortunately, these specific classes encompass an enormous amount of chemistry and biology plus the FFs are continually being developed to increase their applicability – both CHARMM and AMBER need to be able to handle the small organic molecules bound to them while MMFF was also designed with a view to modelling biomolecules although given its extra complexity relative to AMBER and CHARMM, MMFF is seldom used for very large systems.

The computational efficiency of a FF approach also enables simulations of dynamical behaviour—molecular dynamics (MD). In MD, the classical equations of motion for a system of N atoms are solved to generate a search in phase space, or *trajectory*, under specified thermodynamic conditions (e.g. constant temperature or constant pressure). Such a trajectory is important for two reasons. Firstly, it provides configurational and momentum information for each atom from which thermodynamic properties of the system can be calculated. Secondly, the trajectory represents an exploration of the conformation space accessible to a particular system under ‘realistic’ conditions of temperature and pressure.

MD introduces a time dependence. In essence, at any given time, t , the forces, F , on the atoms of mass m moving with velocities v yield accelerations, a , via the simple $F = ma$ equation and thence at a future time $t + \delta t$, a new set of coordinates can be generated where-upon the whole process is repeated. To avoid numerical instability, the time step δt needs to be quite small (~ 1 fs) which places strong limitations on the total simulation time. However, the ability to evolve the system with time and to make contact with thermodynamics are very important. Coupled with its relative efficiency, at least compared to QM, MD is currently the only really viable method for computing the dynamics behaviour of large systems like biomolecules.

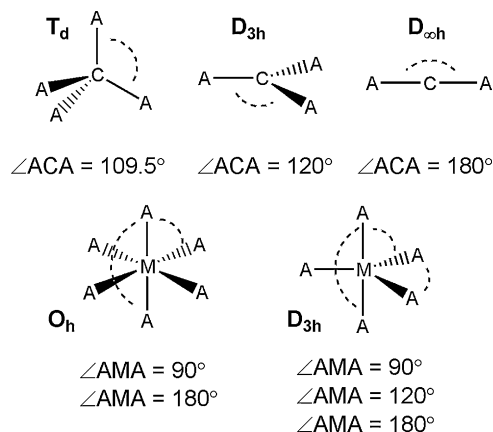


Fig. 11. Valence angles at central atom for various regular geometries.

Consequently, MM and MD have become extremely powerful and useful computational tools for studying a wide variety of chemical and biological problems. However, a significant proportion of real systems also rely on TM centres for their structure and/or function. The presence of TM coordination soon exposes fundamental shortcomings in simple FF equations like (10).

2.2.1. Shortcomings of MM for TM systems

Perhaps the first hurdle encountered in MM for TM complexes is how to describe the angular geometry at the metal centre when using a FF expression like (10). The situation for carbon chemistry is straightforward since the three common geometries – tetrahedral, trigonal planar and linear – are each associated with a single valence angle – 109.5°, 120°, and 180°, respectively. Hence, the reference value, θ_0 , for the bond angle term is clear. In contrast, for common coordination symmetries like octahedral and trigonal bipyramidal, there are multiple reference angles for the same A–M–A triad (Fig. 11).

Landis refers to this as the ‘unique labelling problem’ [41] and while the MM programs of the day could be persuaded to circumvent the problem, this required the definition of “multiple equilibrium positions and redundant atom labelling schemes” resulting in a “tedious over-definition of the molecular topology”.

Many more elegant solutions to this problem have been suggested. A conceptually simple one is based on the Gillespie–Nyholm or valence shell electron pair repulsion (VSEPR) idea that the groups around a central atom will arrange themselves so as to maximise their separation or, equivalently, to minimise their mutual repulsions. Kepert put this essentially ‘points on a sphere’ (POS) approach onto a more quantitative footing by minimising the ligand–ligand repulsion assuming an inverse dependence on the ligand–ligand distance, with powers ranging from 4 to 8, and successfully rationalised the structures of some 5000 main group compounds [42]. Within MM, a POS or ligand–ligand repulsion scheme removes the angle bend term at the metal and thus θ_0 values are not required. This approach has been adopted by Hambley and Comba in their MOMECS program [18]. However, a POS scheme generates the ‘Platonic’ solids – i.e. regular coordination polyhedra – and cannot on its own generate square planar or square pyramidal geometries unless these are enforced by the ligand structure.

The alternative to circumventing the angle bending potential at the metal centre is to replace the harmonic expression in (10) with something more sophisticated. For example, the SHAPES FF [41] uses a Fourier expression for the angular potential which can be designed to produce multiple minima say 90° and 180° as illus-

trated in the original application to square planar low-spin d^8 Rh^I complexes.

Carlsson and Zapata [43] went even further and derived, from the AOM, analytical expressions for the angular potential around metal centres. The functional forms are simple trigonometric functions and depend on the σ or π natures of the ligands which facilitate a calculation of the LFSE. This method is thus a simplification of our ligand field molecular mechanics (LFMM) approach, described in the next section, which calculates the LFSE from a full AOM treatment which requires construction and diagonalisation of V_{LF} . However, despite its promise, the analytical approach outlined by Carlsson and Zapata does not appear to have been developed further and has, to our knowledge, not been incorporated into any molecular modelling software.

2.3. Ligand field molecular mechanics

Ligand field molecular mechanics (LFMM) was first introduced by Burton et al. [26] in 1995. Applications will be discussed in the next section after a brief overview of the methodology.

The central idea of LFMM is to merge conventional MM for the 'organic' parts of a TM complex with an AOM treatment of the LFSE for the metal centre. The LFSE only accounts for the effects of the d electrons and is infinitely negative at zero M–L distances so the FF must include the 'usual' terms for M–L stretching (a Morse function is used) and L–M–L angle bending (a ligand–ligand term is used). The LFSE contribution is thus fully integrated into the MM calculations and the electronic effects feed directly into determining the structure and energy. The LFMM method is therefore distinct from Comba's MM/AOM method [44] which uses a 'pure' MM approach to generate the structure followed by a subsequent AOM calculation to compute various ligand field properties such as d–d spectra and EPR g-values. Both approaches initially ignored electrostatic interactions.

The first LFMM applications focused on σ -only amine donors and assumed a linear dependence of e_σ with bond length, both for the sake of simplicity [26,27]. Ligand–ligand repulsion parameters were based on standard van der Waals terms and energy gradients were computed by finite difference. No special attempt was made to ensure that the AOM parameter values were 'spectroscopically accurate' – i.e. the AOM parameter values from the LFMM are different to those which would be obtained from MM/AOM.

A decade later, the LFMM model was significantly overhauled [45] and a number of new or upgraded features were implemented:

1. a more general functional form was implemented for the distance dependence of the AOM parameters (13);

$$e_\lambda = a_0 + a_1 r + a_2 r^{-2} + a_3 r^{-3} + a_4 r^{-4} + a_5 r^{-5} + a_6 r^{-6} \quad (13)$$

2. the 6–9 van der Waals ligand–ligand repulsion term was replaced by a purely repulsive term, A_{LL}/r^n where usually $n = 6$ for first-row donors or $n = 4$ for second row donors;
3. M–L π bonding was fully implemented including the contributions from forces acting on the 'subsidiary' atoms – i.e. the non-metal atoms connected to the donor atom;
4. an explicit AOM d–s mixing term, e_{ds} , was included to treat the configuration interaction between the valence metal s orbital and the d functions (in D_{4h} $[CuCl_4]^{2-}$, for example, the Cu 4s mixes with $3d_{z^2}$ depressing the latter by about 6000 cm^{-1});
5. the LFSE contributions to the potential energy gradients were computed analytically;
6. electrostatic interactions were added; and
7. the whole model was incorporated into a fully functional molecular modelling package, the Molecular Operating Environment (MOE).

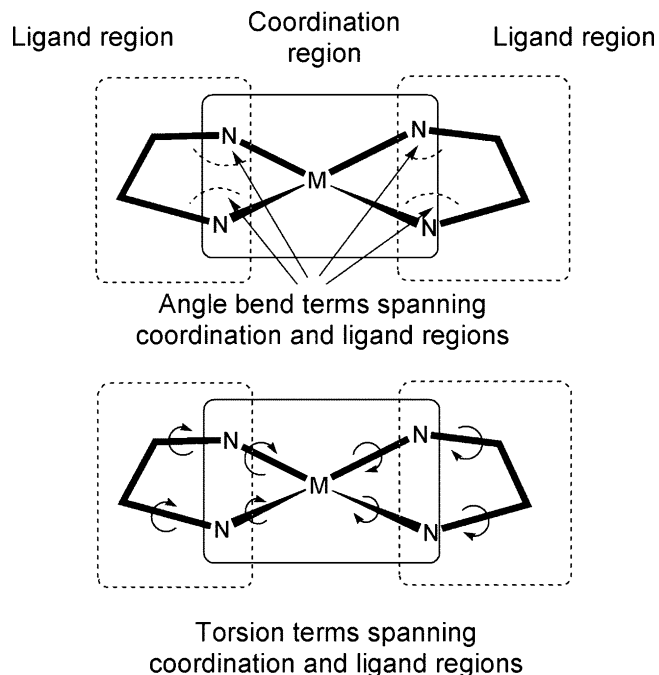


Fig. 12. Schematic representation of division into coordination and ligand regions and force field terms which span the two.

The final point is probably the most significant since it provides a much improved application and development platform.

The new program – d orbital molecular mechanics in MOE (DommiMOE)¹ – was designed to take advantage of existing force fields – e.g. MMFF, AMBER and CHARMM – to describe the ligand. Most of these force fields do not have explicit metal–ligand parameters and those that do are not compatible with LFMM since they do not separate the LFSE and bond stretch contributions (*vide infra*). Hence, the metal is explicitly decoupled from the rest of the molecule.

Each molecule is divided into two overlapping regions as illustrated in Fig. 12 for a $[M(\text{ethylenediamine})_2]^{n+}$ complex. The coordination region contains the metal and its immediately bonded donor atoms (e.g. the MN_4 unit) and the ligand region comprises everything except the metal atom (e.g. the ethylenediamine ligands). The LFMM routines focus on the coordination region and handle the LFSE, M–L bond stretching and L–M–L angle bending although, for the latter, there is no explicit L–M–L angle bending potential, rather the angular geometry is affected by a direct repulsive term between the ligand donor atoms. The MOE FF file treats all the interactions in the ligand region and, using Fig. 12 as an example, is augmented with M–N–C angle, N–M–N–C torsion and M–N–C–C torsion terms which span the coordination and ligand regions. MOE also handles all non-bonding interactions – van der Waals and electrostatic – for the entire molecule.

The construction in Fig. 12 may at first sight seem like that used in QM/MM approaches. However, there are significant differences. Firstly, to the extent that LFMM can be considered QM/MM method at all, the metal is the only 'QM' atom. Hence, the 'QM' region is not the same as the coordination region. Secondly, the 'link' atoms typical of many QM/MM implementations would correspond to the ligand donor atoms. In a 'real' QM/MM calculation, the link atoms are different in the QM and MM regions, typically being H and C

¹ A copy of DommiMOE can be obtained from the authors. Certain conditions apply.

respectively. This construction is not required in the LFMM and there is no 'join'. The LFMM thus provides a uniform, seamless theoretical treatment of the entire molecule.

However, at first sight, there appears to be a 'price' to be paid. Compared to a conventional MM scheme, LFMM has more parameters. In particular, there are up to four AOM parameters – e_{σ} , $e_{\pi x}$, $e_{\pi y}$ and e_{ds} – which have no 'conventional' counterparts. However, the first three are normally fixed with respect to experimental or computed d-orbital energy data for homoleptic systems while e_{ds} acts like a 'switch' and once it exceeds a threshold value, its precise magnitude is less important (see, for example, Section 3.5.3). Hence, in terms of the actual number of parameters which are free to vary, LFMM and conventional MM are comparable especially for FFs like MMFF which use quartic expansion for bond stretching and thus require three parameters just like the Morse function employed in LFMM. This being said, we have yet to automate the parameter-fitting process. Consequently, deriving suitable parameter sets which reproduce, say, experimental and/or DFT structures with an rms deviation in M–L bond lengths of 0.02–0.04 Å and L–M–L bond angles of 2–4° can be a relatively time-consuming business.

3. Applications of LFMM

The magnitude of the LFSE can be significant. In octahedral complexes, values for Δ_{oct} are typically of the order of 10,000–20,000 cm^{−1} and so the stabilisation energy for, say, a low-spin d⁶ Co(III) complex ($-12/5\Delta_{\text{oct}}$) is substantial (120–240 kJ mol^{−1}). Conversely, the LFSE for high-spin d⁵ Mn(II) or Fe(III) is, by construction, zero.

Although the LFMM represents a completely general method for coordination complexes, species at either end of the LFSE extreme can often be well treated by conventional MM – i.e. where the electronic effects of the LFSE are treated implicitly. Indeed, conventional MM may be easier to implement since there are fewer parameters. For example, the Comba group has applied MM to a range of low-spin d⁶ Co(III) complexes [46–49] and since the Co–L interactions are modelled via a simple quadratic function, essentially only two parameters are required per Co–L combination. In contrast, in LFMM, the Morse function, ligand–ligand repulsion, and LFSE all contribute strongly to the Co–L bond length which may require up to six parameters.

Thus, the bulk of the applications of LFMM, and related methods, has been directed at complexes with an intermediate LFSE and especially to strongly Jahn–Teller active species like d⁹ Cu(II) and d⁴ Mn(III) centres for which conventional MM does not provide a general approach. While other groups have normally restricted themselves to simplified σ -bonding only implementations of the LFMM (see Sections 4.1 and 4.2) work from this laboratory includes π bonding and d–s mixing contributions as appropriate. As for the 'organic' part of the FF, well-established parameter sets such as MMFF or MM3 are typically used although we do not consider this aspect in any detail here. The interested reader should consult the primary references for specific information.

3.1. Simple coordination complexes: Cu(II) amines

The first application of the LFMM model was to simple four- and six-coordinate copper(II) amine complexes [27]. These species are invariably planar and tetragonally elongated, respectively – suggestions based on single crystal X-ray diffraction that certain hexacoordinate complexes have regular, undistorted structures turn out to be artefacts of averaging as discussed in Section 3.5.

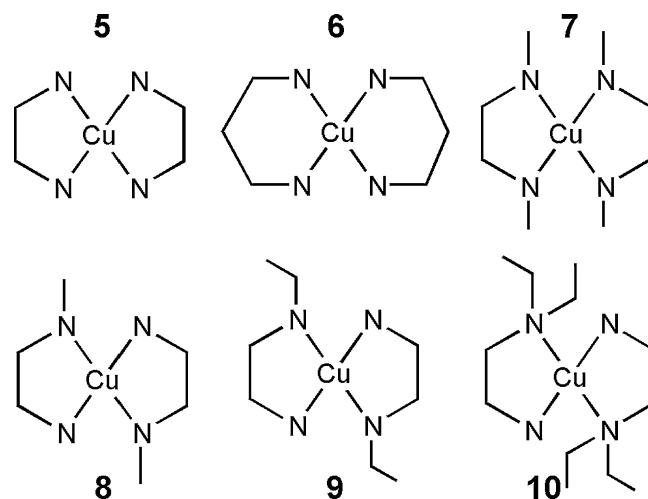


Fig. 13. Structural diagrams for Cu(II) amine complexes.

The structures of the CuN₄ systems result from a competition between ligand–ligand repulsion, which favours tetrahedral coordination, and the LFSE, which favours planar coordination. Clearly, the latter is more important for amine ligation since the experimental and LFMM structures are exclusively planar (Fig. 13 and Table 1).

In addition to predicting a planar coordination for these [CuL₂]²⁺ complexes (L = bidentate amine), the LFMM also describes the steric effects such as the general elongation of the Cu–N bonds for the tetramethyl derivative (7) and the asymmetry between the unsubstituted and substituted nitrogens in the N,N-diethyl complex (10).

The magnitudes of the AOM parameters are estimated from previous ligand field analyses of d–d spectra [50–52]. Hence, for a Cu–N distance of 2.0 Å, $e_{\sigma}(\text{N})$ is around 6000 cm^{−1}.

3.2. [MCl₄]^{2−} complexes

Compared to amines, chloride donors have both smaller e_{σ} values and non-zero e_{π} parameters resulting in an overall weaker ligand field. In addition, ligand–ligand repulsions are relatively more significant for chloride donors than nitrogens. For most complexes containing the [CuCl₄]^{2−} ion, the geometry balances partway between the extremes of planar and tetrahedral. The LFMM automatically generates this 'flattened' structure [45] (Fig. 14).

The flattening of [CuCl₄]^{2−} can also be viewed as a Jahn–Teller distortion of the parent tetrahedral ²T₂ system. In contrast, the ground state for [CoCl₄]^{2−} is ⁴A₂ and is therefore not Jahn–Teller active. The LFMM predicts a perfectly tetrahedral structure. Tetrahedral [NiCl₄]^{2−} is also formally Jahn–Teller unstable with a ³T₁

Table 1

Comparison of calculated and experimental Cu–N bond lengths and chelate bite angles for complexes shown in Fig. 13

Complex	Cu–N (Å) Calc./Exp.	Bite angle (°) Calc./Exp.
5	2.02/2.02	85.4/84.1
6	2.00/2.04	84.8/86.7
7	2.04/2.06	86.7/85.3
8	2.01/2.01 2.04/2.06	86.3/85.9
9	2.03/2.02	86.2/85.0
10	2.02/2.01 2.10/2.08	85.2/87.6

Data from Ref. [27].

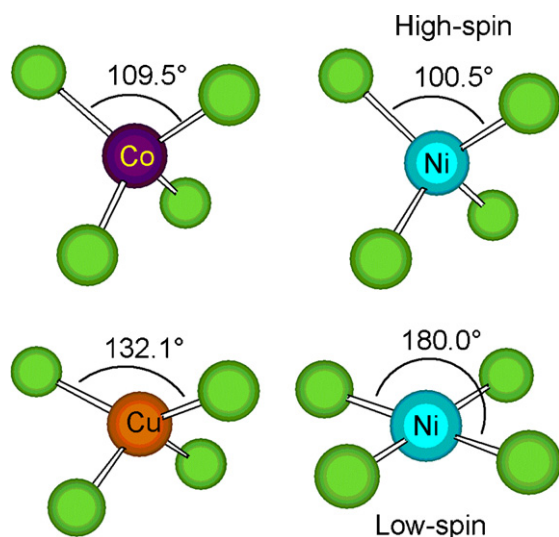


Fig. 14. LFMM structures for $[\text{MCl}_4]^{2-}$ complexes.

ground state but now the LFMM predicts a tetragonally elongated structure (Fig. 14, top right).

The sense of the Jahn–Teller distortions in $[\text{NiCl}_4]^{2-}$ and $[\text{CuCl}_4]^{2-}$ can be interpreted in terms of a simple d-orbital splitting diagram (Fig. 15). A ‘tetragonal’ distortion – i.e. one that maintains D_{2d} symmetry and hence an S_4 axis – splits the t_2 orbitals into a degenerate e set and a non-degenerate b_2 function. Compression raises the b_2 orbital which, in the limit of planar coordination, corresponds to the d_{xy} orbital since the global x and y-axes are rotated 45° relative to the conventional D_{4h} assignment. Elongation lowers b_2 relative to the e set. Thus, in order to avoid generating an orbitally degenerate ground state upon distortion, the d^9 configuration favours compression while the high-spin d^8 configuration favours elongation.

For illustrative purposes, and as a prelude to spin-state effects discussed further in Section 3.6, Fig. 14 also includes the optimised structure for the (hypothetical) low-spin $[\text{NiCl}_4]^{2-}$ complex. The much increased LFSE for a low-spin d^8 configuration now overcomes the ligand–ligand repulsion which results in a planar geometry. Thus we see the spectrum of four-coordinate geometries from regular tetrahedral through to square planar is related to the disposition of the d electrons.

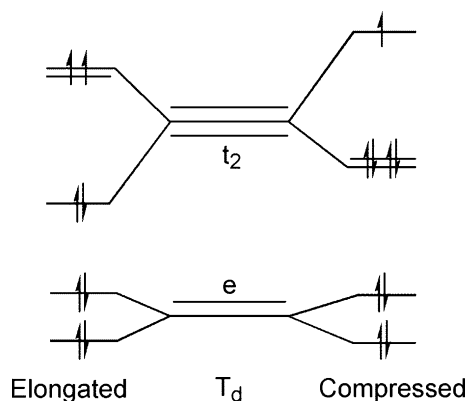


Fig. 15. d-Orbital splitting diagram for tetragonal distortions of a tetrahedral complex.

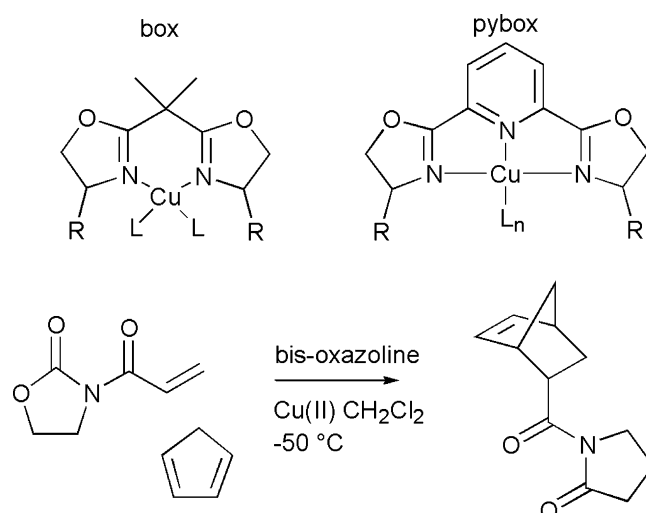


Fig. 16. Generic structural diagrams for copper complexes of box (top left) and pybox (top right) ligands plus the two-point asymmetric Diels–Alder reaction that they catalyse (bottom).

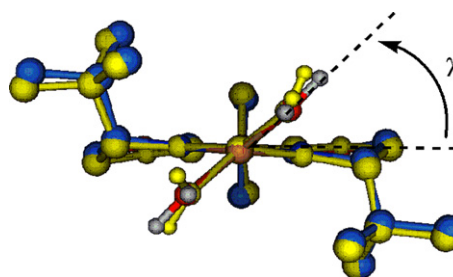


Fig. 17. Definition of twist angle ($^\circ$), χ (top) and overlay of X-ray (yellow) and LFMM structure for $[\text{Cu}\{\text{tb-box}\}(\text{OH}_2)_2]^{2+}$ (bottom).

3.3. Cu(II) bis-oxazoline complexes

The subtle balance between planar and tetrahedral coordination is also seen in Cu(II) bis-oxazoline (box) complexes (Fig. 16) [53]. For example, the diaqua and dichloro complexes of box with $R = \text{'Bu}$ (tb-box) are neither planar nor ‘tetrahedral’. For the former, the twist angles, χ , between the plane of the C_2 -symmetric oxazoline ligand and the CuL_2 plane (Fig. 17) would be zero while for a ‘tetrahedral’ arrangement, they would be 90° . These complexes catalyse the asymmetric Diels–Alder coupling reaction shown in Fig. 16 with the asymmetric induction controlled by the R groups on the oxazoline moieties. Clearly, the predicted asymmetry is reversed for $\chi = 0$ versus $\chi = 90^\circ$.

An LFMM FF for box and pybox ligands was developed based on a set of X-ray crystal structures [53]. The calculated twist angles for $[\text{Cu}\{\text{tb-box}\}\text{L}_2]^{n+}$ ($\text{L} = \text{Cl}$, $n = 0$; $\text{L} = \text{OH}_2$, $n = 2$) agree well with experiment (Table 2).

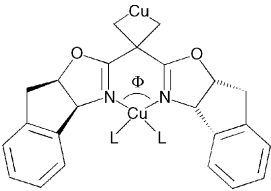
LFMM was then applied to a series of spiro complexes, for which no experimental structural data were available, to try to correlate the observed enantioselectivities with some calculated structural features of the ground state precursor molecules

Table 2
Calculated and experimental twist angles for Cu(II) oxazoline complexes

Complex	χ Calc./exp.
$[\text{Cu}\{\text{tb-box}\}\text{Cl}_2]$	53/52
$[\text{Cu}\{\text{tb-box}\}(\text{OH}_2)_2](\text{O}_3\text{SCF}_3)_2$	30/45
$[\text{Cu}\{\text{tb-box}\}(\text{OH}_2)_2](\text{SF}_6)_2$	30/33

Table 3

Calculated geometrical parameters (diaqua complexes) and experimental enantio- and regio-selectivities



Ligand	Φ	χ	Endo (R)/(S)	Endo:exo
Cyclopropyl-in-box	97.7	19	53:1	44:1
Cyclobutyl-in-box	96.3	18	24:1	38:1
Cyclopentyl-in-box	95.7	20	18:1	37:1
Cyclohexyl-in-box	94.9	22	11:1	26:1

(Table 3). While the correlation between the N–Cu–N bite angle, Φ , and the observed R/S ratio is good for this closely related series, it did not extend very well to other systems which is probably not surprising given that the relatively small selectivity changes mean that the energy differences between the relevant diastereomeric transition states are tiny and that the modelling was based on ground state species.

Subsequently, we attempted to model these systems more completely [54] by replacing the simple equatorial ligands with the actual dieneophile shown in Fig. 16 as well as trying to model the individual diastereomeric transition states for C–C bond formation. This was a ‘pure’ MOE treatment – i.e. not LFMM – where the twist angle was modelled using a torsional term involving rotation about a dummy bond connecting the Cu with the carbon atom bridging the two oxazoline rings while an approximate transition state structure was obtained by using special C–C bond stretch terms based on the optimised distances from DFT TS calculations on a model system with the oxazoline R groups replaced by H. Although the model was able to rationalise the endo–exo selectivity quite well, it still struggled to predict enantioselectivities [54]. A comparable LFMM study has not yet been reported.

3.4. Siderophore complexes: systems with zero LFSE

At the other LFSE extreme are those systems for which it is rigorously zero. Under these circumstances, the LFMM becomes ‘conventional’ but it is still advantageous by virtue of the implementation in MOE. A wide selection of popular force fields are distributed with MOE and are all expressed in a common format. For example, the bond-stretch and angle bend terms in MOE are coded for a quartic expansion. The bond stretching term is shown in (14) and it can mimic both the simple harmonic form used in AMBER and CHARMM plus the more complicated quartic expansion used in MMFF94 (15), where kb_{ij} is the force constant (md/Å), Δr_{ij} is the difference between the actual and reference bond lengths and $cs = -2 \text{ Å}^{-1}$ [34]. The advantage for the LFMM is that M–L parameters developed within a particular FF are transferable to any of the others and the process usually only entails renaming the relevant atom types.

$$E_{\text{str}} = k_{ij}(r_{ij} - r_{0,ij})^2 + k'_{ij}(r_{ij} - r_{0,ij})^3 + k''_{ij}(r_{ij} - r_{0,ij})^4 \quad (14)$$

$$E_{\text{str}}(\text{MMFF94}) = 143.9325 \frac{kb_{ij}}{2} \Delta r_{ij}^2 \times \left(\frac{1 + cs \Delta r_{ij} + 7}{12cs^2 \Delta r_{ij}^2} \right) \quad (15)$$

Many bacteria secrete compounds called siderophores specifically to sequester iron either from the environment or other organisms. Siderophores show extremely high affinities for Fe^{3+}

with binding constants for bacterial species of the order of $\log \beta > 30$ [55].

Streptomyces coelicolor produces a tris-hydroxamate tetrapeptide coelichelin with four stereocentres in the peptide chain. The putative peptides were identified via genome mining [56] although their stereochemistries were ambiguous. Since only tiny quantities of coelichelin could be isolated, single crystals were not available and so the structure could not be confirmed by X-ray diffraction. Consequently, a series of NMR experiments were undertaken. Complexing the molecule facilitates the structure elucidation but the natural choice of Fe^{3+} is strongly paramagnetic, hence the Ga^{3+} complex is used instead since the structures of Fe^{3+} and Ga^{3+} complexes are very similar and Ga^{3+} is diamagnetic.

While not technically a transition metal, for the purposes of LFMM modelling, Ga^{3+} and high-spin Fe^{3+} are essentially comparable since both have formally zero LFSEs. LFMM parameters were developed on the basis of limited X-ray structural data augmented by density functional theory calculations. Thirteen constraints were derived from the NMR experiments – five H–H distances and eight H–C–C–H torsions – and compared to those predicted by computing all possible isomers of $[\text{Ga}(\text{coelichelin})]$. Note that the NMR constraints were not enforced on the calculations. This contrasts with the typical use of NMR constraints which are usually explicitly included to restrain the geometry. Only one combination of chiral centres gave uniform, simultaneous agreement with all the experimental constraints (Fig. 18).

3.5. Jahn–Teller effects in six-coordinate Cu(II) complexes

Six-coordinate d^9 copper(II) complexes invariably display large tetragonal distortions from octahedral symmetry with the vast

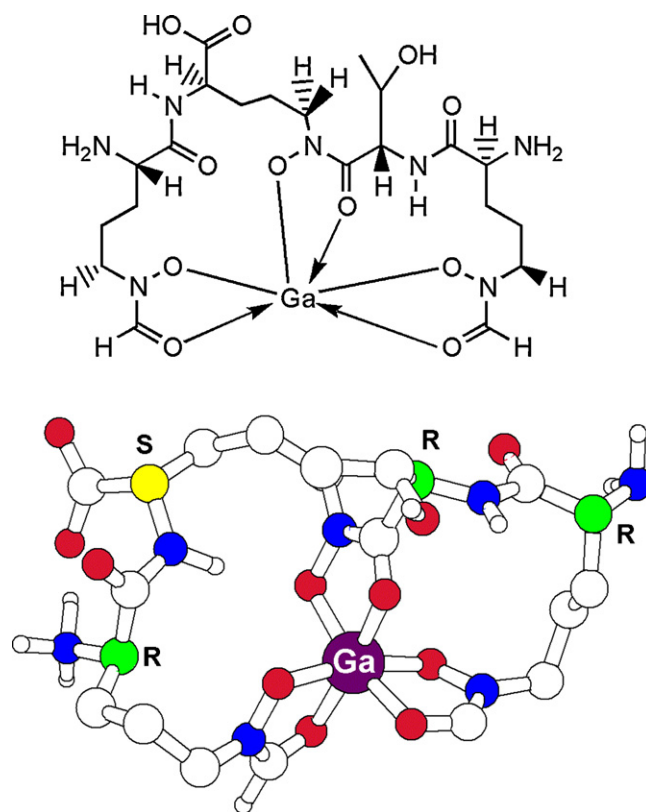


Fig. 18. Structural diagram of $[\text{Ga}(\text{coelichelin})]$ (top) and the calculated structure which best reproduced the NMR constraints (bottom). Non-polar hydrogens omitted for clarity. The peptide chiral centres are labelled R or S as appropriate.

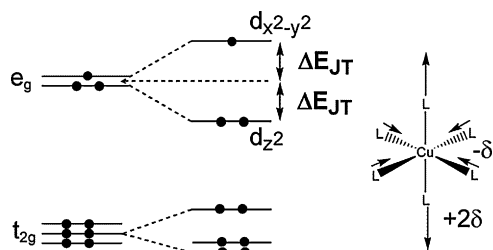


Fig. 19. Schematic representation of the d-orbital energy changes accompanying a tetragonal Jahn–Teller elongation of an octahedral Cu(II) complex.

majority being tetragonally elongated. This observation can be rationalised on the basis of the d electron stabilisation energy (Fig. 19). The geometric distortion raises the original 2E_g degeneracy of the parent octahedral system such that there are two stabilising electrons in d_{z^2} versus a single destabilising electron in $d_{x^2-y^2}$. The net lowering of the electronic energy by ΔE_{JT} drives the distortion but is resisted by the vibrational potential which is a minimum at the octahedral geometry. When these two forces are in balance, a stable structure results.

Fig. 19 shows an elongation along the z-axis but this is clearly only part of the complete picture.

3.5.1. The Mexican hat potential energy surface

In the absence of external perturbations, an octahedral CuL_6 species could equally well elongate along the x- or the y-axes. These possibilities are accommodated in the more complex diagram shown in Fig. 20 [29].

In O_h symmetry, the Jahn–Teller-active vibration, Q , is doubly degenerate with modes Q_θ and Q_ϵ (Fig. 20, bottom). In order to display the energy as a function of two vibrational modes, a three-dimensional figure is necessary. The so-called ‘Mexican hat

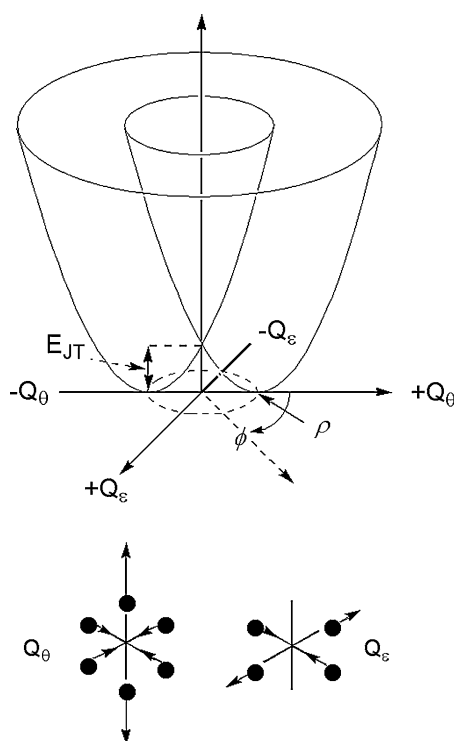


Fig. 20. First-order Jahn–Teller potential energy surface—the Mexican hat.

potential surface’ is commonly used (Fig. 20, top) with the proportions of the two modes determined by the mixing parameter, ϕ . The Q_θ mode generates the ‘normal’ elongation along z but suitable combinations of both modes generate the other elongated structures, plus compressed geometries plus all the intervening rhombic structures.

To first order – i.e. a harmonic vibrational potential and a linear relationship between the Jahn–Teller energy and the vibrational displacement (linear vibronic coupling) – all these structures are equienergetic. However, this feature is lost to second-order since the vibrational mode is anharmonic, the vibronic coupling is non-linear and as soon as the symmetry becomes less than O_h there is the possibility of d–s mixing which preferentially stabilises one of the d orbitals.

The effect of d–s mixing can be illustrated in tetragonal D_{4h} symmetry where the metal d_{z^2} and valence s orbital both transform as a_{1g} and may therefore mix. In planar $[\text{CuCl}_4]^{2-}$, detailed low temperature single crystal electronic absorption experiments have established that the d_{z^2} orbital is about 6000 cm^{-1} lower than predicted based on simple AOM calculations which include just the chloride e_σ and e_π parameters [57].

3.5.2. The warped Mexican hat

In the context of the Jahn–Teller effect, the second-order terms differentiate between elongated and compressed structures. They have about the same magnitudes with both anharmonicity and d–s mixing favouring elongation while second-order electronic effects favour compression [29]. On balance, therefore, tetragonal elongation is lower in energy which leads to a ‘warping’ of the Mexican hat surface.

The warping is quite a subtle effect. Fig. 21 displays representations of the path along the bottom of the PE surface as a function of the Q_θ/Q_ϵ mixing parameter, ϕ , for three possible scenarios. In an isotropic environment (Fig. 21, top), all three elongation axes are equally likely and hence each local minimum is equally occupied. Significantly, although each individual molecule is elongated, any time-averaged structural technique, in particular single-crystal X-ray diffraction, would appear to report a regular octahedron. In contrast, spectroscopy – e.g. EXAFS or d–d electronic absorption – would detect the underlying distorted structure. Thus, while the room temperature X-ray structure of $[\text{Cu}(\text{tach})_2](\text{NO}_3)_2$ (tach = 1,3,5-triaminocyclohexane) shows essentially six equal Cu–N distances, the perchlorate salt has a ‘normal’ elongated structure [58]. The d–d spectra of both complexes are the same and show

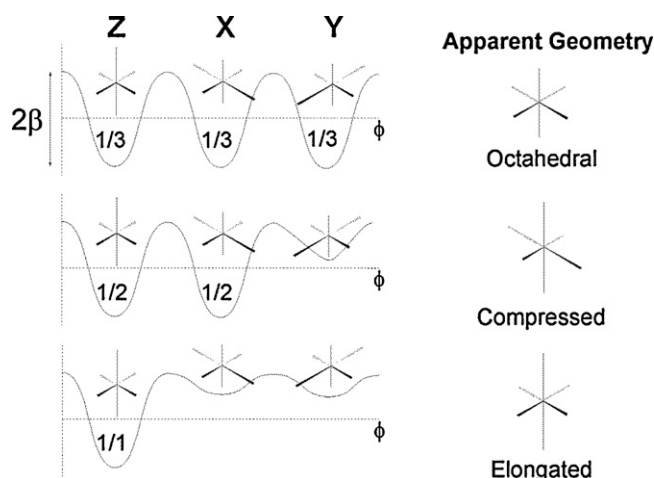


Fig. 21. Warping of Mexican hat PE surface.

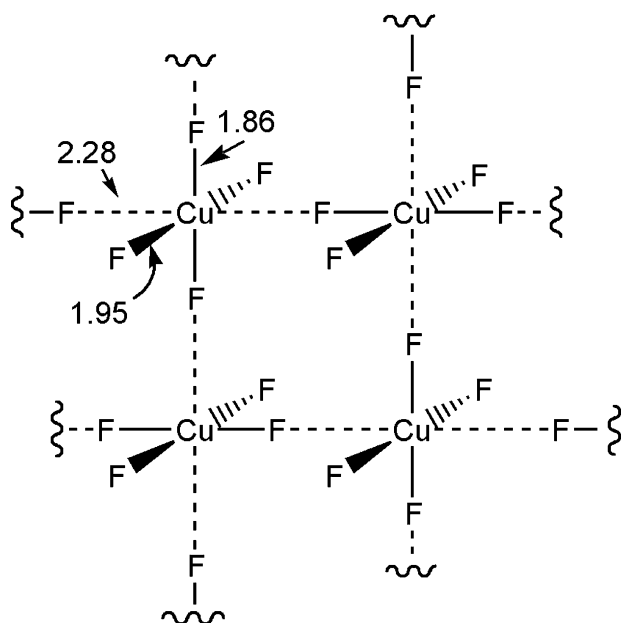


Fig. 22. Diagram of the arrangement of the CuF_6 polyhedra in the (001) plane of K_2CuF_4 (after Fig. 4 of Ref. [60]).

two absorption maxima consistent with the underlying tetragonal structure.

The second scenario is when two wells are occupied while the third is essentially unoccupied (Fig. 21, middle). Here, the averaged structure would appear to be tetragonally compressed as was originally reported for K_2CuF_4 [59] with four longer Cu–F bonds of 2.08 Å and two shorter contacts at 1.95 Å. However, these data were based on an incorrect space group, presumably due to the relatively crude instrumentation available in 1959. Subsequent investigation by Reinen and Krause [60] established the true structure as comprising interchanging elongated structures oriented at 90° as shown in Fig. 22.

The final, and most common, scenario (Fig. 21, bottom) is where the environment and/or the ligand result in one well being significantly more stable than the other two (or possibly, there being only one minimum). This results in the ‘conventional’ elongated structure.

Where more than one elongation is possible, there is an intervening transition state with a compressed geometry. The barrier, 2β , between successive wells (Fig. 21) determines the dynamics of the system. If the barrier is significantly lower than kT then the complex is free to ‘hop’ from one well to the next – the dynamic Jahn–Teller effect. If the barrier is significantly larger than kT , then the complexes are ‘frozen’ in their respective wells – the static Jahn–Teller effect. The dynamic behaviour is thus temperature dependent. Indeed, the earlier example of apparently octahedral $[\text{Cu}(\text{tach})_2](\text{NO}_3)_2$ oscillates between two minima just above the phase transition temperature of 120 K and below this, reverts to a classic ‘static’ elongated system.

3.5.3. Theoretical treatment of the Jahn–Teller effect in Cu(II) species

Capturing all this complexity is a challenge for theory. On the one hand, there is the thorny issue about whether it is theoretically justifiable to use ‘normal’ computational approaches at all. The models tend to assume the Born–Oppenheimer approximation which does not apply where there is significant vibronic coupling [61]. However, in practice, it appears that providing we move away from the

octahedral singularity, ‘normal’ QM and MM methods appear to work quite well.

On the other hand, the energetics are significant but subtle. To first order (i.e. the harmonic approximation), the first d–d transition corresponds to $4\Delta E_{\text{JT}}$ which, for Cu(II) complexes with typical band energies of 6000–9000 cm^{-1} , corresponds to $\Delta E_{\text{JT}} \sim 17$ to 27 kJ mol^{-1} . Thus, the distorted structure is significantly more stable than the octahedral precursor. A second-order treatment further distinguishes elongated from compressed geometries but the energy differences are only a fraction of ΔE_{JT} . For example, variable temperature EPR experiments place the barrier height, 2β , in $[\text{Cu}(\text{tach})_2]^{2+}$ at around 300 cm^{-1} ($\sim 4 \text{ kJ mol}^{-1}$).

The very first application of the LFMM included the Jahn–Teller distortions of some simple hexacoordinate Cu(II) complexes [27]. This study has recently been significantly extended and enhanced [62].

Seventeen six-coordinate Cu(II) complexes of nitrogen donor ligands were selected as a training set (Fig. 23) based on the criterion that the species with the largest possible Jahn–Teller distortion will suffer the smallest crystallographic ‘averaging’ errors.

The comparison between the crystallographic and LFMM structures is shown in Fig. 24 which displays the average Cu–N distance at the top and the difference between the averaged Cu–N(axial) and averaged Cu–N(equatorial) distances. The agreement is generally excellent.

A significant feature of LFMM for these complexes is d–s mixing. Since the vibrations are anharmonic and the electronic term non-linear, d–s mixing plays the deciding role in stabilising elongated over compressed geometries. The e_{ds} parameters acts like a switch in that it needs to exceed a certain threshold before the elongated structure becomes lower in energy.

3.5.4. Barriers between successive elongations

As mentioned in the previous section, the barrier, 2β , between successive elongated geometries can be of the order of kT and can therefore be measured experimentally via, for example, variable temperature EPR. However, since the intrinsic barrier is relatively small, the behaviour of a given complex can dramatically depend on the crystal environment. For example, the perchlorate salt of $[\text{Cu}(\text{tach})_2]^{2+}$ has a ‘normal’ elongated structure at room temperature while the nitrate salt displays six almost equal Cu–N bond lengths at 300 K. However, variable temperature EPR measurements on the latter down to 4 K show dynamic Jahn–Teller behaviour at room temperature with a phase transition to static behaviour at 120 K [58]. The EPR measurements establish 2β at around 300 cm^{-1} .

Standard MM codes are designed to locate local minima efficiently. The compressed tetragonal structures for (most) Cu(II) complexes are first-order saddle points, or transition states (TSs), and will not be automatically located unless special modifications are made such as in Warshel’s empirical valence bond (EVB), Truhlar’s multiconfiguration MM (MCM), or Goddard’s ReaxFF methods [63–65]. However, for simple homoleptic complexes like $[\text{Cu}(\text{tach})_2]^{2+}$ it is relatively straightforward to locate the TS manually.

A series of constrained LFMM calculations where the axial bond is fixed at progressively shorter distances eventually leads to a structure with two short and four long Cu–N contacts. Significantly, the energy difference between the compressed TS and the elongated structure is $\sim 270 \text{ cm}^{-1}$, in excellent agreement with experiment, plus the application of a uniaxial strain does not force the structure through an ‘octahedral’ geometry but instead

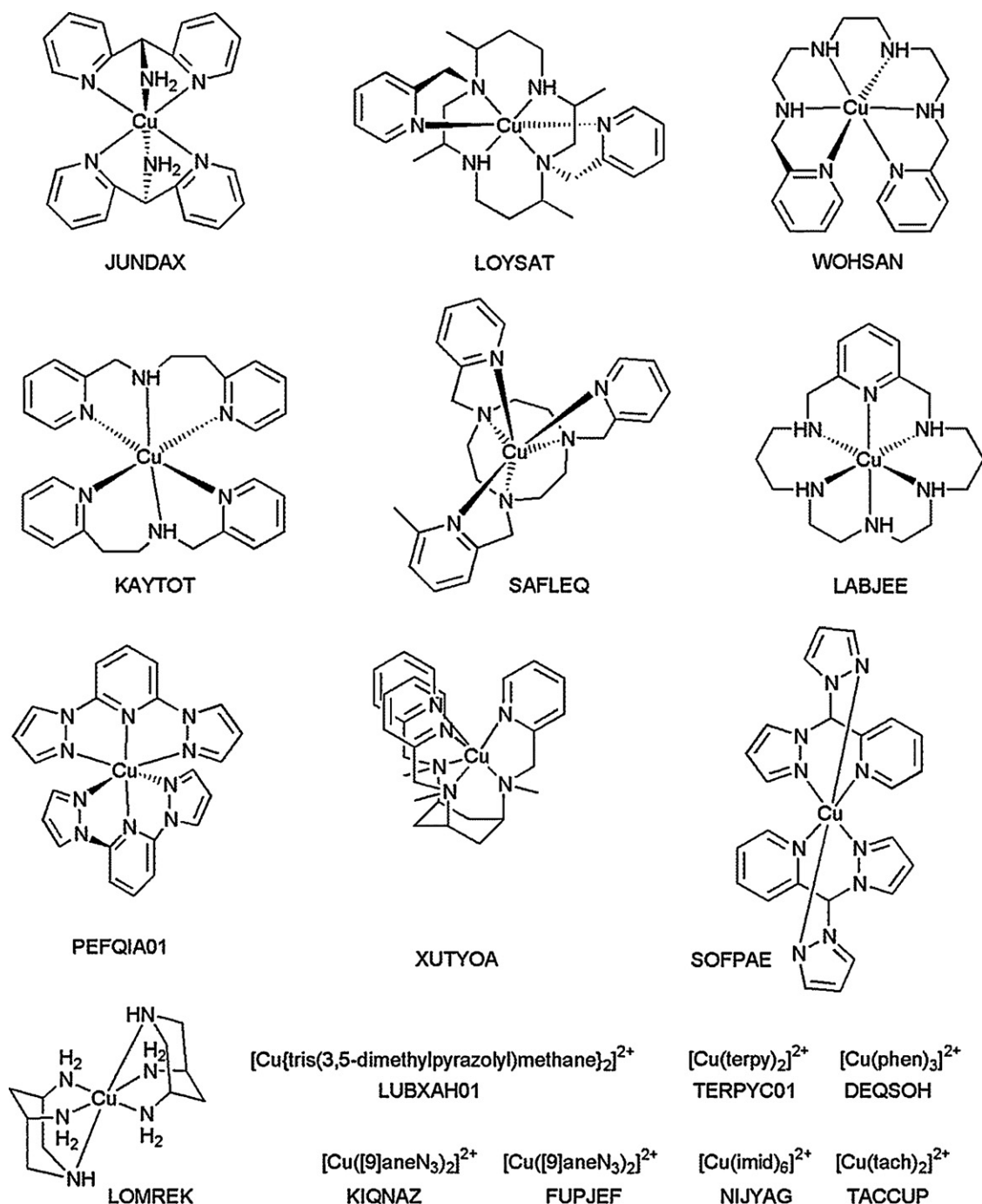


Fig. 23. Training set of Cu(II) complexes for LFMM treatment of Jahn–Teller distortions. Cambridge Structural Database refcodes are included.

a series of rhombic structures. The LFMM thus correctly follows the ‘valley floor’ of the warped Mexican hat PE surface (Fig. 25).

Further suitable experimental data are sparse since most of the temperature dependent studies have been carried out on doped systems where the structures of the Cu(II) centres are heavily influenced by the host lattice and are unknown in detail anyway. However, by way of illustration, 2β barriers were also computed for $[\text{Cu}(\text{NH}_3)_6]^{2+}$ and $[\text{Cu}(\text{terpy})_2]^{2+}$ (terpy = terpyridyl). These complexes were chosen since the former has no ligand constraints to Jahn–Teller elongation while the latter comprises meridionally coordinated tridentate donors which are more constrained than

tach. This is consistent with the computed barriers of 1100 and 215 cm^{-1} respectively.

3.5.5. Truly compressed complexes

Compressed six-coordinate Cu(II) species doped into diamagnetic host lattices, typically of Zn(II), have been observed spectroscopically. However, pure Cu(II) complexes with compressed geometries are much rarer. Nevertheless, the relatively low barriers between successive elongated geometries in ‘normal’ complexes of only a few kJ mol^{-1} prompted Halcrow et al. [24] to look for ligand systems which might be able to stabilise a compressed structure preferentially.

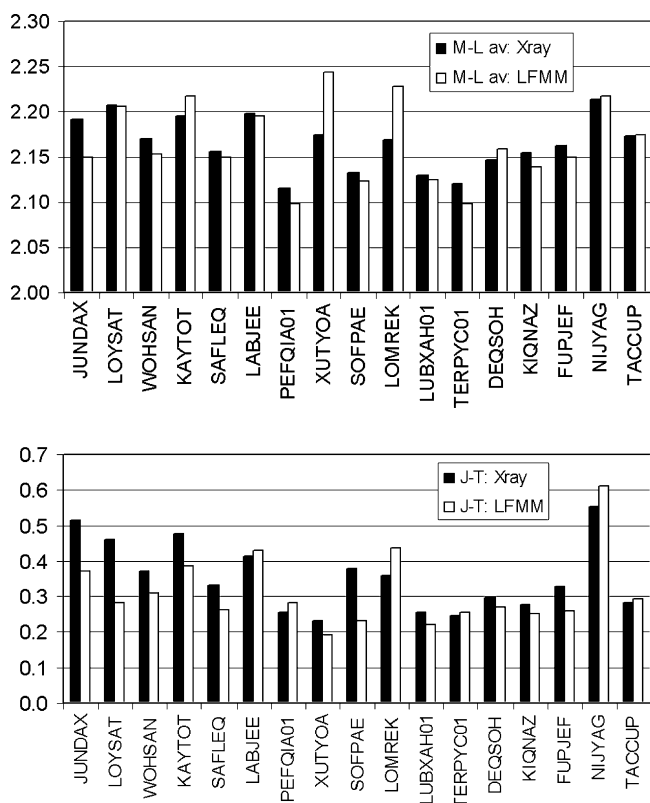


Fig. 24. Comparison of LFMM (white bars) and experimental (black bars) structural data (Å) for complexes sketched in Fig. 23.

The tridentate, meridionally coordinating ligands shown in Fig. 26 and Table 4 can generate elongated and compressed structures, depending on the steric demands of the R substituents.

A combination of crystallography and spectroscopy was used to assign the structure as either compressed or elongated and the LFMM-optimised structures (Table 4) are in excellent qualitative agreement. Significantly, the LFMM parameterisation was based exclusively on elongated structures.

3.5.6. Cu(II) Jahn–Teller effects: summary

The previous sections establish that the LFMM describes the features of the entire Mexican hat potential energy surface for a single d^9 Cu(II) complex to remarkably good accuracy. This is a significant achievement given that the AOM parameters were

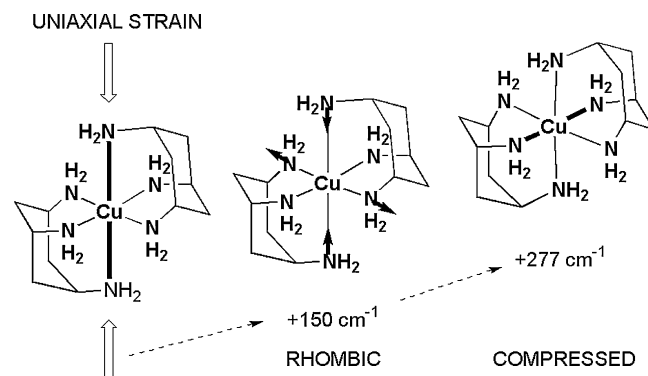


Fig. 25. Schematic representation of effect of applying uniaxial strain to $[\text{Cu}(\text{tach})_2]^{2+}$. The initial effect is a rhombic distortion (middle) leading to the compressed geometry (right).

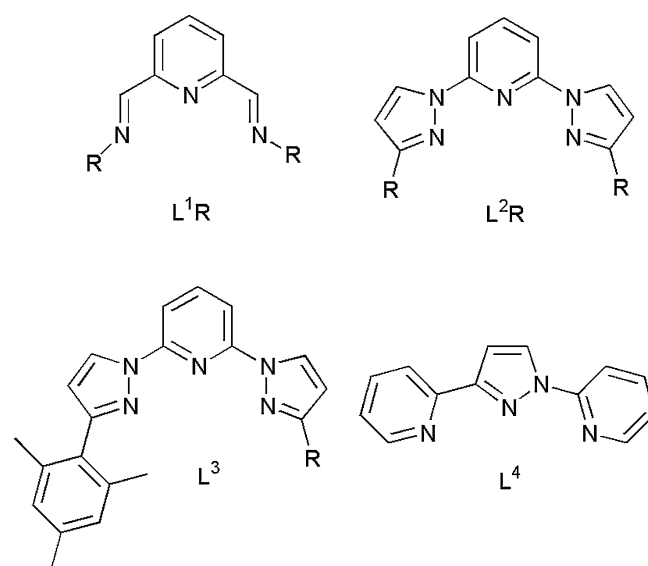


Fig. 26. Tridentate ligands designed by Halcrow to explore preferential stabilisation of truly compressed Cu(II) complexes.

based largely on previous studies of the d–d spectra [50] while the other LFMM parameters were determined by reproducing the (solid state) structural data. Furthermore, no special information concerning compressed species was included and yet the model handles both their structures and relative energies. The final ques-

Table 4

Experimentally assigned ground state and LFMM-optimised bond lengths (Å) for complexes based on the ligands shown in Fig. 26

Complex	Exp ground state	LFMM M–L(av) r_x, r_y, r_z	LFMM Geometry
$[\text{Cu}(\text{L}^2\text{H})_2][\text{BF}_4]_2$	$\{d_{y^2-z^2}\}$	2.29, 2.11, 1.90	Elongated
$[\text{Cu}(\text{L}^2\text{Ph})_2][\text{BF}_4]_2$	d_{z^2}	2.24, 2.19, 1.90	Rhombic (compressed)
$[\text{Cu}(\text{L}^2\text{Mes})_2][\text{ClO}_4]_2$	d_{z^2}	2.22, 2.21, 1.88	Compressed
$[\text{Cu}(\text{L}^2\text{iPr})_2]^{2+}$	–	2.25, 2.19, 1.90	Rhombic (compressed)
$[\text{Cu}(\text{L}^2\text{tBu})_2]^{2+}$	–	2.38, 2.38, 1.90	Compressed
$[\text{Cu}(\text{L}^2\text{CF}_3)_2]^{2+}$	–	2.25, 2.19, 1.90	Rhombic (compressed)
$\alpha\text{-}[\text{Cu}(\text{L}^3)][\text{ClO}_4]_2$	$\{d_{y^2-z^2}\}$	2.28, 2.14, 1.90	Rhombic (elongated)
$[\text{Cu}(\text{L}^1\text{Cy})_2][\text{BF}_4]_2$	$\{d_{y^2-z^2}\}$	2.38, 2.06, 1.91	Elongated
$[\text{Cu}(\text{L}^1\text{tBu})_2][\text{BF}_4]_2$	d_{z^2}	2.34, 2.34, 1.92	Compressed
$[\text{Cu}(\text{L}^1\text{NH}_2)_2][\text{ClO}_4]_2$	d_{z^2} (RT) $\{d_{y^2-z^2}\}$ (5 K)	2.30, 2.03, 1.93	Elongated
$[\text{Cu}(\text{L}^1\text{OH})_2][\text{ClO}_4]_2$	d_{z^2} (RT) $\{d_{y^2-z^2}\}$ (low temp)	2.29, 2.02, 1.93	Elongated
$[\text{Cu}(\text{L}^4)_2][\text{ClO}_4]_2$	d_{z^2}	2.37, 2.15, 1.82	Rhombic (compressed)

The non-standard d orbital designation $d_{y^2-z^2}$ is adopted to retain a single axis frame definition for both ground states where the z direction coincides with the Cu–N vector to the central donor atoms of the tridentate ligands.

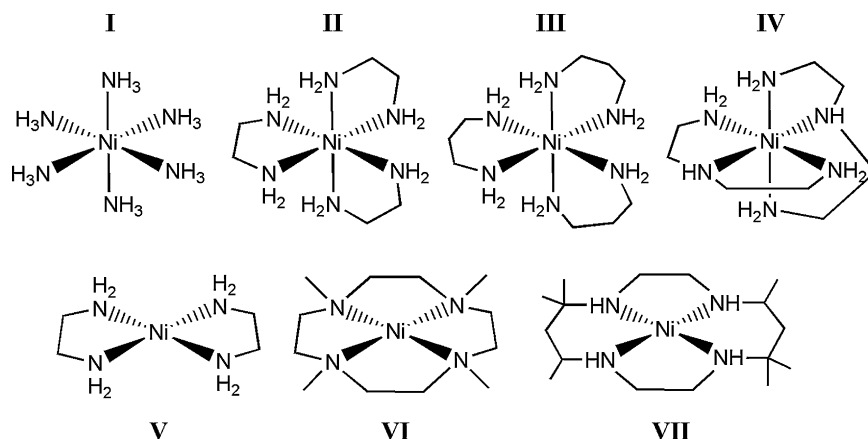


Fig. 27. Selection of six- and four-coordinate Ni(II) amine complexes modelled using an early version of LFMM (Ref. [26]). Selected structural data are shown.

tion would be whether the LFMM treatment could treat the packing effects present in the actual crystal structure but these calculations have not yet been attempted.

3.6. Spin-state effects

A minor modification of Fig. 19 where $d_{x^2-y^2}$ is completely empty generates a (hypothetical) octahedral low-spin d^8 system where the stabilisation energy is doubled relative to a d^9 configuration with a concomitant increase in the tetragonal distortion to the extent that the axial ligands are lost completely. Thus, the square planar geometry of low-spin d^8 systems has an LFSE origin [29].

The original LFMM paper [26] considered both octahedral, high-spin and planar, low-spin d^8 Ni(II) amine complexes, a selection of which is shown in Fig. 27. The average Ni–N distances for the two spin states are significantly different (~ 0.2 Å, see Table 5). However, in contrast to previous applications of conventional MM where two independent sets of parameters were required [19], the ability to populate the d-orbitals in either a high-spin or low-spin configuration results in a single set of LFMM parameters for both spin states. However, while a successful model for structures, this early application of LFMM did not address the relative energies of different spin states.

Table 5

Comparison of LFMM and experimental metric data for Ni(II) complexes shown in Fig. 27

Complex ^b	Ni–N ^a (Å)		N–Ni–N ^a (°)	
	Calc.	Obs.	Calc.	Obs.
I	2.12	2.13	90	90
			180	180
II	2.12	2.13	81.8	81.9
			173.1	171.8
III	2.14	2.15	83.8	86.9
			173.1	175.8
IV	2.05	2.06	81.7	81.6
	2.15	2.16	168.0	167.3
V	1.94	1.92	87.6	86.4
			179.7	180.0
VI	1.99	1.98	90.3	90.6
			167.4	168.6
VII	1.98	1.96	90.0	90.0
			180.0	180.0

Data from Table 2 of Ref. [26].

^a Averaged bond lengths and angles.

^b Structural diagrams in Fig. 27.

The LFSE is, by construction, always negative and thus favours a low-spin configuration. Countering this is the d–d interelectronic repulsion energy which always favours the high spin state. Interelectronic repulsion can be considered either in terms of the ‘spin-pairing’ energy or, probably more correctly, as an electronic exchange effect. Spin-pairing ‘costs’ energy thus favouring high spin states; exchange occurs between electrons of the same spin hence high-spin states have more exchange stabilisation. Either way, the final spin state is a balance between the one-electron stabilisation and the two-electron interelectronic repulsion terms.

A full, many-electron ligand field treatment often, and especially for first-row TMs, assumes the Russell–Saunders coupling scheme where the d-electron spin and orbital angular momenta are independent [66]. The spin–orbit coupling necessary for calculating magnetic properties is added subsequently. The d–d interelectronic repulsion is parameterised within either the Condon–Shortley scheme (with parameters F_2 and F_4) or the Racah scheme (with parameters B and C). The latter is more popular [2] since for spin-allowed d–d transitions, only B is required. However, in a ‘full-basis’ treatment using all the many-electron terms derived from the given d^n configuration, the schemes are equivalent and there is a simple relationship between the parameters (16).

$$B = F_2 - 5F_4; \quad C = 35F_4 \quad (16)$$

In principle, the LFSE could be expressed using many-electron terms which, given suitable values for the interelectronic repulsion parameters, would allow the method to predict the spin state automatically. This is the philosophy behind the effective Hamiltonian approach developed by Tchougreff (see Section 4.3). However, given the significantly more complex mathematical problem of expressing the LFSE and its derivatives with respect to many-electron terms, plus the added computational burden of inverting larger matrices – the $d^{2/8}$, $d^{3/7}$, $d^{4/6}$ and d^5 configurations are, respectively, 45, 120, 210 and 252-fold degenerate – we adopted a simpler, more pragmatic approach of treating the effective interelectronic repulsion energy via a simple, bond-length-dependent penalty function.

A ‘proof of concept’ study was undertaken for Co(III) fluoride and cyanide complexes [67]. To our knowledge, $[\text{CoF}_6]^{3-}$ is the only homoleptic high-spin complex of d^6 Co(III) while $[\text{Co}(\text{CN})_6]^{3-}$ is certainly low-spin. LFMM parameters for both high- and low-spin forms of each complex were developed with the aid of DFT calculations. For example, DFT-optimised Co–L bond lengths for the ground state complexes plus the hypothetical low-spin $[\text{CoF}_6]^{3-}$ and high-spin $[\text{Co}(\text{CN})_6]^{3-}$ species were part of the target data for the FF parameters. In addition for these complexes, a comparison

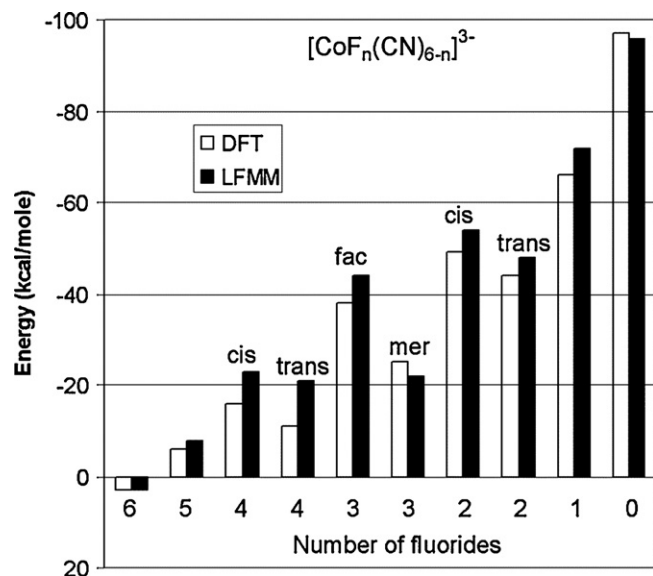


Fig. 28. Comparison of calculated spin-state energy differences for $[\text{CoF}_n(\text{CN})_{6-n}]^{3-}$ complexes.

of LFT predictions with DFT indicated the latter gives a reasonable spin-state energy difference (see Ref. [67] for details) and was subsequently used to map out the spin-state energy difference, ΔE_{spin} for each complex as a function of the Co–L distance. The structures of all the mixed-ligand systems $[\text{CoF}_n(\text{CN})_{6-n}]^{3-}$, $n = 1–5$, were then computed by both LFMM and DFT and the energies of the former empirically corrected for spin state effects using the spin-state energy differences, ΔE_{spin} , expressed on a per-ligand basis derived from the homoleptic complexes.

As shown in Fig. 28, the agreement between DFT and LFMM is satisfactory. However, a shortcoming of this study is that the spin-state effects are not incorporated into the optimisation and so do not directly influence the structure. The Co(III) systems are sufficiently simple that this approximation is satisfactory but a more general scheme would include interelectronic repulsion contributions to the energy gradients. This has been reported for octahedral $[\text{Ni}(\text{NH}_3)_6]^{2+}$ and the hypothetical low-spin planar $[\text{Ni}(\text{NH}_3)_4]^{2+}$ system where, given the existing parameters for the high-spin systems, a simple penalty function of the same form as (13) has been tuned to reproduce the (DFT-optimised) Ni–N distance for the low-spin complex [68]. In principle, therefore, LFMM can model both spin states with a single parameter set and therefore be used to predict which spin state is lowest in energy. No conventional MM approach can emulate this since separate FFs are required for each spin. However, we await a more exhaustive appraisal of LFMM spin-state effects.

3.7. Type 1 copper enzymes

The Type 1 (T1) ‘blue’ copper enzymes are responsible for a range of redox processes in biological systems [69]. For example, plastocyanin (Pc) is involved in plant photosynthesis while azurin (Az) participates in bacterial photosynthesis.

Compared to ‘normal’ copper complexes, the T1 active site (Fig. 29) possesses a number of unusual structural and spectroscopic features [70]:

- a distorted tetrahedral (or trigonal bipyramidal) structure with a strong Cu–thiolate bond even in the oxidised form plus a long thioether or carbonyl oxygen contact;

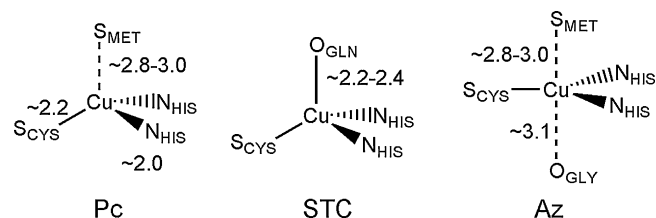


Fig. 29. Schematic representations of T1 active site structures of plastocyanin (Pc), stellacyanin (STC) and azurin (Az).

- a very intense charge transfer transition around 600 nm;
- relatively high redox potentials;
- in the EPR spectra of the oxidised Cu(II) form, there is an unusually low copper hyperfine coupling in the g_{\parallel} region.

The T1 active site appears to have features of both ‘normal’ Cu(II) and Cu(I) complexes. For example, oxidised copper is often planar four-coordinate with an N_4 donor set while d^{10} Cu(I) is often tetrahedral and, as a softer metal, prefers second row donors like sulphur. Given its role in electron transfer (ET) and the expectation from Marcus theory that efficient ET is associated with a small reorganisation energy, λ , the idea that the protein somehow enforces the structure around the metal centre to minimise λ became very popular.

This ‘entatic state’ [71] (or rack [72]) model is certainly appealing and prompted Ryde to try and calculate its magnitude using DFT [73]. However, B3LYP optimisation of a model for the T1 active site in Pc gave basically the same coordination geometry at the metal centre as that reported in the full protein structure. Ryde et al. [73] were forced to the unexpected and somewhat controversial conclusion that the geometry in oxidised T1 centres is not under any protein strain. Instead, the structure is dominated by the strong Cu–thiolate bond.

The combined electronic effects of the d^9 configuration and Cu–thiolate binding present some significant challenges for LFMM [74,75]. We begin with the presumption that although protein molecules may be large and complex, they form simple M–L coordinate bonds – i.e. a Cu–N(imidazole) bond can be handled in exactly the same way irrespective of whether it corresponds to an isolated imidazole or to a histidine. However, in order to parameterise the enzyme system, we require information on the specific types of bonds involved which is straightforward for imidazole coordination, where significant experimental data are available, but difficult for thiolate and thioether bonds where experimental data on small-molecule systems are sparse or absent.

We resort, therefore, to using DFT calculations on model homoleptic species as a basis for developing LFMM parameters (Table 6). Hence, as shown in the box in Fig. 30, LFMM parameters are developed for the homoleptic complexes which reproduce the DFT-optimised Cu–L distances and L–Cu–L angles. The parameters are then applied unaltered to the same active-site model used by Ryde et al. [73] in their DFT study.

The good agreement between LFMM and DFT once again confirms that the LFMM behaves just like DFT in its ability to

Table 6
Cu–L bond lengths (Å) for species shown in Fig. 30

Compound	Cu–N	Cu–S (thioether)	Cu–S (thiolate)
$[\text{Cu}(\text{imidazole})_4]^{2+}$	1.99/2.00		
$[\text{Cu}(\text{DMS})_4]^{2+}$		2.37/2.35	
$[\text{Cu}(\text{SMe})_4]^{2-}$			2.32/2.33
$[\text{Cu}(\text{SMe})(\text{imidazole})_2(\text{DMS})]^+$	2.02/2.04	2.90/2.70	2.14/2.16

First entry is LFMM, second is DFT.

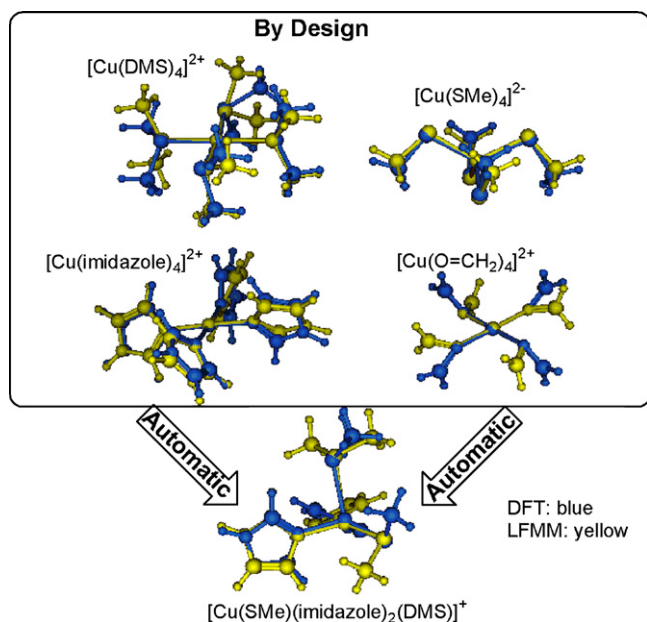


Fig. 30. Species used to develop LFMM parameters for T1 centres.

capture M–L bonding electronic effects. Furthermore, just as in six-coordinate complexes (Section 3.5.3), d–s mixing plays a pivotal role. There are two stable forms of the T1 active site model – the lower energy trigonal one shown in Fig. 30 and a higher energy, essentially planar form. DFT calculations [76] suggest a delicate energy balance with the trigonal model being more stable. Interestingly, a comparable LFMM result is only obtained once the e_{ds} value for the Cu–S(thiolate) bond exceeds a threshold value. Once again, d–s mixing acts like an electronic ‘switch’.

The LFMM was applied to 24 crystallographically characterised proteins [75] and an rmsd in the Cu–L bond lengths of 0.11 Å and 8° in L–Cu–L bond angles achieved – i.e. the LFMM and PDB results are basically the same within experimental uncertainty.

A comparison of structures representative of the three active site types shown in Fig. 29 is given in Fig. 31, Tables 7 and 8.

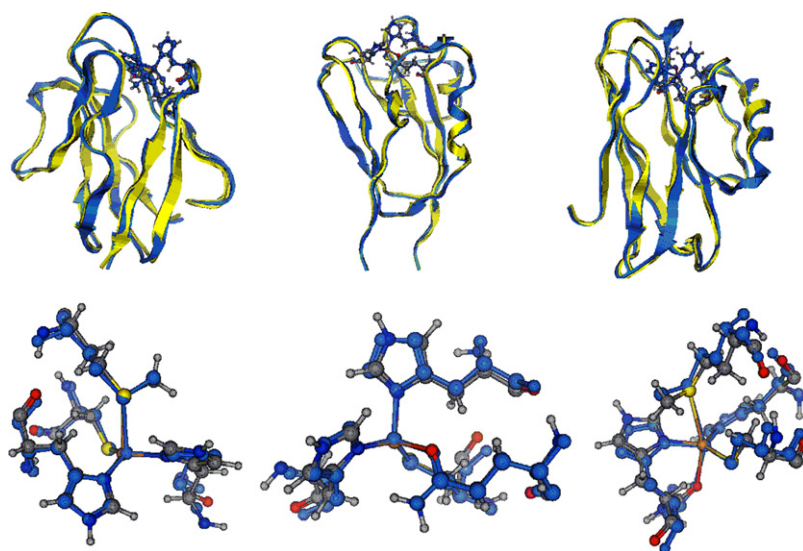


Fig. 31. Rmsd overlays of experimental (blue) and computed (yellow or CPK) backbone carbons (top) and active sites (bottom) for Amicyanin (left), Stellacyanin (middle) and Azurin (right) (PDB codes 1AAC, 1JER, 1DYZ). The solvent layer is omitted for clarity.

Table 7

Comparison of PDB and LFMM Cu–L bond lengths (Å) for complete proteins shown in Fig. 31

1AAC	PDB	LFMM	1JER	PDB	LFMM	1DYZ	PDB	LFMM
HIS53	1.954	2.029	HIS46	1.960	2.045	GLY45	2.720	2.666
CYS92	2.108	2.148	CYS89	2.178	2.176	HIS46	2.040	2.014
HIS95	2.033	2.023	HIS94	2.043	2.028	CYS112	2.135	2.184
MET98	2.904	2.859	GLN99	2.209	2.253	HIS117	1.988	2.062
						MET121	3.260	2.924

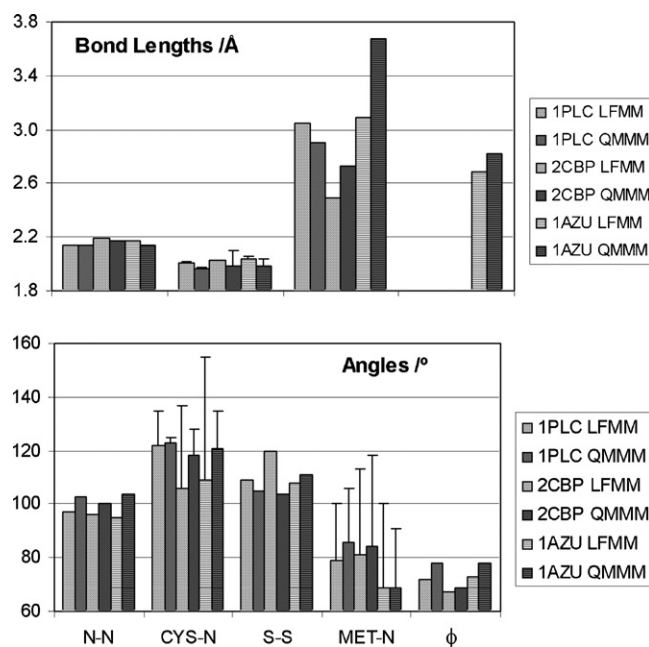


Fig. 32. Comparison of LFMM (lighter bars) and QM/MM (darker bars) metrics for selected T1 sites. PLC = plastocyanin; CBP = cucumber basic protein; AZU = azurin. ϕ is the angle between the CuN_2 and CuS_2 planes.

The quality of the LFMM results can also be assessed with respect to comparable QM/MM calculations [77] (Fig. 32). In both instances, explicit solvent is included and again, the agreement is good. The fact that the LFMM data were obtained several orders of magnitude

Table 8Comparison of PDB and LFMM bond angles ($^{\circ}$) at the metal centre for the proteins shown in Fig. 31

1AAC	PDB	LFMM	1JER	PDB	LFMM	1DYZ	PDB	LFMM
HIS53–CYS92	136	141	HIS46–CYS89	133	139	GLY45–HIS46	78	82
HIS53–HIS95	104	97	HIS46–HIS94	101	98	GLY45–CYS112	104	98
HIS53–MET98	84	86	HIS46–GLN99	94	87	GLY45–HIS117	86	83
CYS92–HIS95	112	108	CYS89–HIS94	117	113	GLY45–MET121	148	156
CYS92–MET98	110	112	CYS89–GLN99	101	112	HIS46–CYS112	132	140
HIS95–MET98	100	104	HIS94–GLN99	101	95	HIS46–HIS117	106	103
						HIS46–MET121	73	75
						CYS112–HIS117	121	116
						CYS112–MET121	105	105
						HIS117–MET121	88	92

faster than the QM/MM results bodes well for using the LFMM for molecular dynamics simulations.

3.8. Dinuclear copper centres

Another common copper enzyme active site is the dinuclear Type 3 centre (Fig. 33) which is implicated in O_2 transport and activation [69]. The fully oxidised T3 site is an attractive target for LFMM since it combines the electronic activity of d^9 centres with the first attempt at modelling both multi-nuclear species and complexes with bridging ligands [78].

In contrast to the T1 centre, several crystallographically characterised structural models for the T3 site are available (Fig. 34) from which an LFMM treatment was developed.

The AOM calculation underpinning the LFSE presumes independent metal centres. Thus, the extension of the LFMM to multi-metal centres could be problematic if the metals were strongly coupled. However, for the model test system $[\{Cu(NH_3)_3\}_2-\mu-O_2]^{2+}$, and the dinuclear species shown in Fig. 34, the particular combination of electronic configuration and geometry ensures that the gradient of the LFSE is dominated by the highest energy combination of d functions which mirrors the situation in the mono-nuclear model species $[Cu(NH_3)_3(O_2)]$ and thus the ‘isolated metal’ approach remains satisfactory in the dinuclear systems [78].

An important feature of the dinuclear complexes is that the $[Cu_2O_2]^{2+}$ subunit prefers to be planar, i.e. the folding angle shown in Fig. 35 is 180° . This is implicitly accounted for in the LFMM by defining the Cu–O π -bonding directions relative to the second copper centre rather than the other oxygen atom. One of the originally perceived advantages of the LFMM was the explicit treatment of separate σ and π bonding effects via the AOM e_{σ} and e_{π} parameters [26] and here we see a powerful demonstration of this feature.

The LFMM is in generally good agreement both with experimental and DFT data (Fig. 36) [78]. The agreement extends to the energies (relative to DFT) of the structures within about 12 kJ mol^{-1} of the overall lowest. The exception is **14** where the LFMM and

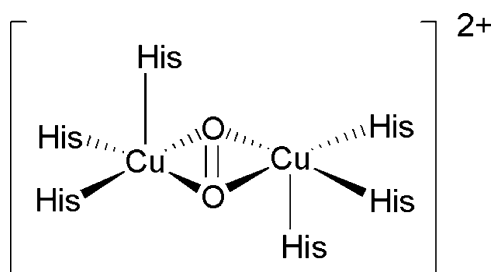


Fig. 33. Schematic representation of fully oxidised T3 active site with bound peroxido ligand.

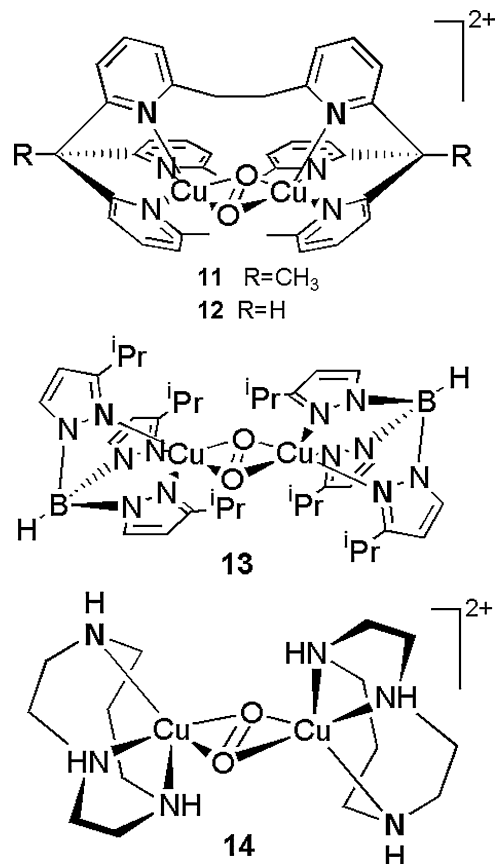


Fig. 34. Dinuclear Cu complexes as structural models for the T3 active site.

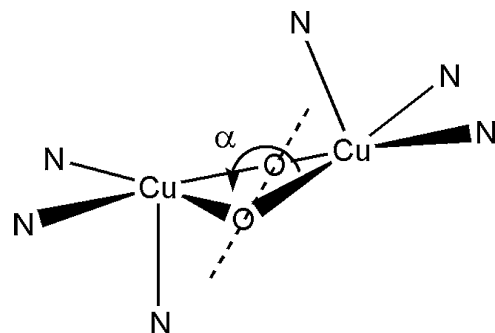


Fig. 35. Definition of folding angle, α , about the O–O vector in dinuclear complexes.

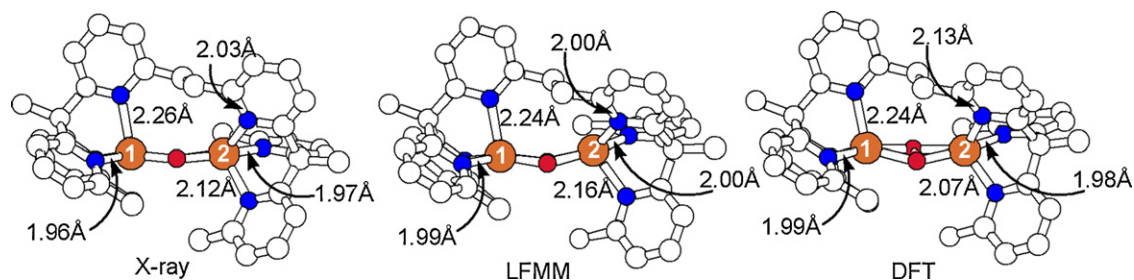


Fig. 36. Observed X-ray structure (left), LFMM-computed structure (centre) and DFT-optimised geometry (right) for 11 showing Cu–N distances. All comparable structural data for the X-ray and LFMM versions of 12 are virtually the same. H atoms omitted for clarity.

DFT energies disagree substantially but this is traced to a generic shortcoming in the ‘organic’ force field treatment of the macrocyclic ligand.

In common with previous LFMM applications to five-coordinate Cu(II) species [26], we see strong apical elongations. Significantly, the demands of a particular ligand can make the two copper centres different, a feature which also figures in enzymes like tyrosinase. However, the application of LFMM to the protein system has not yet been reported.

4. Other approaches

While steady, if somewhat laborious, development of LFMM has occurred, the level of activity in force field approaches for TM systems has, since the mid 1990s, tapered off significantly. We suppose at least two possible reasons for this. Firstly, attempts to develop a general approach based purely on conventional MM struggled. For example, Gajewski et al. [79] reported a ‘general’ scheme based on MM2 parameters but were only able to achieve ‘moderately good reproducibility of structures’ plus they acknowledged the need for the kind of LFSE term included in LFMM viz: ‘If deviations in distances, angles, or torsions are in evidence, then specific electronic interactions should perhaps be pursued’.

A second possible reason for the ‘slow-down’ in FF development for TM systems is the advent of QM/MM. QM/MM circumvents the problem of how to treat the metal centre parametrically. It is probably also significant that QM/MM provides a ready route into modelling reaction mechanism [80]. Of course, suitably formulated and parameterised MM can also treat reaction pathways (e.g. EVB [81], ReaxFF [65], MCFF [64]) including modelling transition states for processes involving TMs (Q2FF [82]). However, these methods, just like LFMM, are not yet ‘mainstream’. In contrast, the availability of QM/MM in the most popular quantum chemical codes (e.g. Gaussian, ADF, Jaguar) plus software packages like ChemShell, which allow the user to combine their favourite MM and QM codes, ensures an increasingly widespread application of QM/MM [80]. No doubt, the ever increasing speed and power of hardware contributes substantially.

Nevertheless, there are a few schemes which are either directly descended from LFMM or adopt a similar philosophy – i.e. the direct incorporation of d-electron effects into the energy and gradients of the MM optimisation. These are discussed briefly in the following sections. Note that the preceding criterion excludes the MM/AOM method [44] which, although undoubtedly useful, generally relies on ‘conventional’ MM for structure and treats the ligand field part subsequently as an ‘add-on’. However, there are two notable extensions of MM/AOM. The first is the treatment of Jahn–Teller distortions in six-coordinate Cu(II) complexes where the effect of an energy term based on the expressions developed by Deeth and Hitchman [29] is included in the calculation as a con-

straint imposed via Lagrangian multipliers [83]. Elongation along each of the three possible axes can be explored individually. However, the energy expression is for amine systems only and assumes tetragonal symmetry.

The second is the inclusion of electronic effects in MM/AOM by modifying the AOM parameters to reflect ‘bent bonding’ [84]. Thus, the angle θ between the Cu–L vector and the predicted direction of the sp^3 hybrid of an amine donor is used to moderate the value of e_σ assuming a $\cos^6 \theta$ dependence. While this change does not figure in the geometry optimisation, it does generate improved estimates of the subsequent ligand field properties like d–d transition energies.

4.1. SIBFA-LF

The extension of the sum of interactions between fragments *ab initio* (SIBFA) method to include an LFSE contribution is a direct descendant of LFMM and was joint venture between the LFMM group of the present author and the SIBFA group of Gresh and Giessner-Prettre. SIBFA-LF [85] incorporates elements of the same LFSE code as in DommiMOE although, to date, only the σ -bonding capability has been implemented.

SIBFA [86] implements a polarisable FF with metal–ligand energetics designed to mimic interaction energies obtained from quantum chemical calculations typically at the MP2 level. The extended version, SIBFA-LF [85], has been applied to Cu(II) complexes of water, imidazole and a few other simple ligands and shown to give improved structures over ‘normal’ SIBFA although given the way that SIBFA is parameterised, the M–L bonding energetics can be designed to be ‘correct’ even when the structure is not. Hence, the Cu–imidazole interaction energies for [Cu(imidazole)₄]²⁺, which in ‘normal’ SIBFA is tetrahedral, agree with the MP2 estimates and while the SIBFA-LF structure is more planar, the interaction energies are unchanged. However, despite this promising start, there do not appear to have been any further applications of SIBFA-LF.

4.2. GULP

A similar extension to that for SIBFA has also been implemented into the general utility lattice program (GULP) for modelling extended solids [87]. Again, a σ -only implementation of the AOM LFSE was incorporated and applied to systems containing the strongly Jahn–Teller active high-spin d⁴ Mn(III) centre in Mn₂O₃ and LaMnO₃ systems. Crystallographically, these systems are reported to contain both regular and distorted MnO₆ sites which the enhanced theoretical approach was able to reproduce. However, just as for SIBFA-LF, the ligand-field-extended version of GULP seems to have been applied only to this single series of compounds.

4.3. Effective crystal field and deductive molecular mechanics

The final method we discuss is the effective crystal field (ECF) approach of Tchougreff and coworkers [88–90]. The philosophy of the ECF method is similar to the LFMM in that, at its heart, the ECF uses a crystal/ligand field calculation to compute the energies of the d states. However, there are significant differences:

- in the ECF model, the external potential, V_{LF} , is generated from a semi-empirical MO calculation of the ligand functions; in LFMM, V_{LF} is a function of the AOM parameters and is therefore entirely parametric;
- in the ECF model, the many-electron energy levels derived from the full set of functions arising from the d^n configuration are calculated, albeit with a parametric treatment of inter-electronic repulsion. The ECF approach thus accounts for the spin state automatically. In LFMM, only the one-electron (i.e. d orbital) energies are computed. Interelectronic repulsion is treated approximately via a distance-dependent penalty function based on high-spin/low-spin energy or structural differences (see Section 3.6).

The ECF approach thus represents the generalisation of the LFMM to a full d^n basis. The authors apply their method to some relatively simple complexes and achieve impressive accuracy both in terms of the optimised structures and the prediction of the ground spin states for Fe(II) and Co(II) complexes of N donor ligands.

Tchougreff has also recently published a theoretical analysis which relates the quantum mechanical description of quite subtle bonding features like *cis* and *trans* influences to a comparable classical MM formulation [91]. By using the elements of the one-electron density matrix as an economical set of electronic structure variables for the closest ligand shell, a way of obtaining suitable classical expressions and parameters is described—the so-called deductive molecular mechanics (DMM) model. We await actual implementation and application of the method to TM complexes.

5. Conclusions

The structural, spectroscopic and magnetic properties of Werner-type coordination complexes are profoundly affected by the d electrons. They also result in complicated electronic states, which from a theoretical perspective, appear to demand a full quantum mechanical treatment. Yet, despite the ever-increasing speed and power of modern digital computers, QM treatments of TM systems are relatively compute-intensive. Long simulation periods or screening of large numbers of small molecules are, and will remain, intractable.

In contrast, ligand field theory, which is specifically designed for d states, is computationally efficient. Over the last half-century or so it has also been shown to provide a reasonable, if semi-quantitative, description of the nature of metal ligand bonding. The addition of an explicit LF-based d-electron-energy term to the conventional MM potential energy expression captures most of the essential physics around the metal centre. Coupling this with a term to treat d–d interelectron repulsion, either phenomenologically as in LFMM or within the full d^n basis treatment of ECF, further improves the method such that MM is able to provide a treatment comparable to full QM but at a much reduced computational cost.

The all-important LFSE can be based on the angular overlap model which, being bond centered, is ideally suited for incorporation into MM. Aside from providing a general framework within which to treat TM centres, LFMM accurately describes a number

of significant electronic effects which are omitted in conventional MM:

- the full Mexican hat potential energy surface describing the Jahn–Teller effect in six-coordinate d^9 Cu(II) complexes;
- the ability to treat multiple spin states of Co(III) and Ni(II) complexes with a single set of parameters and thus be able to use LFMM to predict the lowest energy spin state;
- the effects of explicit d–s mixing in tetragonal Cu(II) complexes plus the trigonal geometry of the Type I active site in blue copper proteins;
- the explicit M–L π effects necessary to keep the $[\text{Cu}_2\text{O}_2]^{2+}$ core of Type 3 copper model complexes planar.

All of these examples have been tested against comparable DFT treatments and shown to produce at least as good a result and sometimes an even better one. An empirical approach offers some distinct advantages over QM in that experimental data can also be used to inform the parameterisation.

This review has focused almost exclusively on the LFMM studies arising from our group. Since the introduction of the LFMM in 1995, only a few others have implemented this type of approach. The absence of new development is probably due to two factors. The first is that the LFMM requires a certain amount of new code development. The second is that DFT in general, and QM/MM in particular, promise to solve many problems without requiring any tedious parameter development. This lack of parameters plus no readily available software has further hampered the cause.

However, the outlook for the future is encouraging. As the number of applications to new and diverse problems in coordination, bioinorganic and catalytic chemistry grows, we hope to inspire others to use methods like LFMM. Of course, not all problems will be well suited to the method—the exploration of reaction mechanisms springs readily to mind. Nevertheless, there are many other problems for which an LFMM approach is well suited (molecular dynamics, conformational searching, virtual high-throughput screening) and thus we hope that the LFMM can be viewed as a complementary computational technique. So far, the LFMM method has worked well in a reasonably diverse range of applications. The issue thus comes down to whether the benefits of appreciably faster calculations outweigh the initial time investment to develop suitable parameters. To this end, a more efficient, automated parameter optimisation would be of enormous use.

References

- [1] D.A. Johnson, P.G. Nelson, *Inorg. Chem.* 34 (1995) 5666.
- [2] C.J. Ballhausen, *Introduction to Ligand Field Theory*, McGraw-Hill, New York, 1962.
- [3] H.A. Bethe, *Ann. Phys.* 3 (1929) 133.
- [4] M. Gerloch, R.G. Woolley, *Prog. Inorg. Chem.* 31 (1983) 371.
- [5] M. Gerloch, R.G. Woolley, *J. Chem. Soc., Dalton Trans.* (1981) 1714.
- [6] A.J. Bridgeman, M. Gerloch, *Prog. Inorg. Chem.* 45 (1997) 179.
- [7] B.N. Figgis, M.A. Hitchman, *Ligand Field Theory and Its Applications*, John Wiley and Sons Ltd., New York, 2000.
- [8] D.A. Johnson, P.G. Nelson, *Inorg. Chem.* 38 (1999) 4949.
- [9] R.K. Hocking, R.J. Deeth, T.W. Hambley, *Inorg. Chem.* 46 (2007) 8238.
- [10] T. Ziegler, J. Autschbach, *Chem. Rev.* 105 (2005) 2695.
- [11] P.E.M. Siegbahn, M.R.A. Blomberg, *Chem. Rev.* 100 (2000) 421.
- [12] N.E. Schultz, Y. Zhao, D.G. Truhlar, *J. Phys. Chem. A* 109 (2005) 11127.
- [13] A.J. Boone, M.G. Cory, M.J. Scott, M.C. Zerner, N.G.J. Richards, *Inorg. Chem.* 40 (2001) 1837.
- [14] D.M. Ball, C. Buda, A.M. Gillespie, D.P. White, T.R. Cundari, *Inorg. Chem.* 41 (2002) 152.
- [15] J.J.P. Stewart, *J. Mol. Mod.* 13 (2007) 1173.
- [16] H. Kayi, T. Clark, *J. Mol. Mod.* 13 (2007) 965.
- [17] R.J. Deeth, *Coord. Chem. Rev.* 212 (2001) 11.
- [18] P. Comba, T.W. Hambley, *Molecular Modeling of Inorganic Compounds*, VCH, Weinheim, 1995.
- [19] R.D. Hancock, *Prog. Inorg. Chem.* 37 (1989) 187.

- [20] M. Reiher, O. Salomon, B.A. Hess, *Theor. Chem. Acc.* 107 (2001) 48.
- [21] O. Salomon, M. Reiher, B.A. Hess, *J. Chem. Phys.* 117 (2002) 4729.
- [22] R.J. Deeth, N. Fey, *J. Comp. Chem.* 25 (2004) 1840.
- [23] A. Ghosh, *J. Biol. Inorg. Chem.* 11 (2006) 712.
- [24] M.A. Halcrow, *Dalton Trans.* (2003) 4375.
- [25] J.M. Holland, X.M. Liu, J.P. Zhao, F.E. Mabbs, C.A. Kilner, M. Thornton-Pett, M.A. Halcrow, *J. Chem. Soc., Dalton Trans.* (2000) 3316.
- [26] V.J. Burton, R.J. Deeth, C.M. Kemp, P.J. Gilbert, *J. Am. Chem. Soc.* 117 (1995) 8407.
- [27] V.J. Burton, R.J. Deeth, *J. Chem. Soc., Chem. Commun.* (1995) 573.
- [28] M.A. Hitchman, *Inorg. Chem.* 21 (1982) 821.
- [29] R.J. Deeth, M.A. Hitchman, *Inorg. Chem.* 25 (1986) 1225.
- [30] C.E. Schaeffer, C.K. Jorgensen, *Mol. Phys.* 9 (1965) 401.
- [31] R.J. Deeth, M.A. Hitchman, G. Lehmann, H. Sachs, *Inorg. Chem.* 23 (1984) 1310.
- [32] R.J. Deeth, C.M. Kemp, *J. Chem. Soc., Dalton Trans.* (1992) 2013.
- [33] M. Gerloch, R.C. Slade, *Ligand-Field Parameters*, Cambridge University Press, Cambridge, 1973.
- [34] T.A. Halgren, *J. Comput. Chem.* 17 (1996) 490.
- [35] T.A. Halgren, *J. Comput. Chem.* 17 (1996) 520.
- [36] T.A. Halgren, *J. Comput. Chem.* 17 (1996) 553.
- [37] T.A. Halgren, R.B. Nachbar, *J. Comput. Chem.* 17 (1996) 587.
- [38] A.K. Rappe, C.J. Casewit, K.S. Colwell, W.A. Goddard, W.M. Skiff, *J. Am. Chem. Soc.* 114 (1992) 10024.
- [39] D.A. Pearlman, D.A. Case, J.W. Caldwell, W.S. Ross, T.E. Cheatham, S. Debolt, D. Ferguson, G. Seibel, P. Kollman, *Comput. Phys. Commun.* 91 (1995) 1.
- [40] B.R. Brooks, R.E. Bruccoleri, B.D. Olafson, D.J. States, S. Swaminathan, M. Karplus, *J. Comput. Chem.* 4 (1983) 187.
- [41] V.S. Allured, C.M. Kelly, C.R. Landis, *J. Am. Chem. Soc.* 113 (1991) 1.
- [42] D.L. Kepert, *Inorganic Stereochemistry*, Springer-Verlag, Berlin/Heidelberg/New York, 1982.
- [43] A.E. Carlsson, S. Zapata, *Biophys. J.* 81 (2001) 1.
- [44] P. Comba, T.W. Hambley, M.A. Hitchman, H. Strateimer, *Inorg. Chem.* 34 (1995) 3903.
- [45] R.J. Deeth, N. Fey, B.J. Williams-Hubbard, *J. Comp. Chem.* 26 (2005) 123.
- [46] J. Bartol, P. Comba, M. Melter, M. Zimmer, *J. Comput. Chem.* 20 (1999) 1549.
- [47] P. Comba, A.F. Sickmuller, *Inorg. Chem.* 36 (1997) 4500.
- [48] P. Comba, A.F. Sickmuller, *Angew. Chem. Int. Ed. Eng.* 36 (1997) 2006.
- [49] P. Comba, H. Jakob, B. Nuber, B.K. Keppler, *Inorg. Chem.* 33 (1994) 3396.
- [50] R.J. Deeth, M. Gerloch, *Inorg. Chem.* 23 (1984) 3846.
- [51] R.J. Deeth, M. Gerloch, *Inorg. Chem.* 24 (1985) 1754.
- [52] R.J. Deeth, M. Gerloch, *J. Chem. Soc., Dalton Trans.* (1986) 1531.
- [53] I.W. Davies, R.J. Deeth, R.D. Larsen, P.J. Reider, *Tetrahedron Lett.* 40 (1999) 1233.
- [54] R.J. Deeth, N. Fey, *Organometallics* 23 (2004) 1042.
- [55] S. Dhungana, J.M. Harrington, P. Gebhardt, U. Moellmann, A.L. Crumbliss, *Inorg. Chem.* 46 (2007) 8362.
- [56] S. Lautru, R.J. Deeth, L.M. Bailey, G.L. Challis, *Nat. Chem. Biol.* 1 (2005) 265.
- [57] M.A. Hitchman, P.J. Cassidy, *Inorg. Chem.* 18 (1979) 1745.
- [58] J.H. Ammeter, H.B. Burgi, E. Gamp, V. Meyer-Sandrin, W.P. Jensen, *Inorg. Chem.* 18 (1979) 733.
- [59] K. Knox, *J. Chem. Phys.* 30 (1959) 991.
- [60] D. Reinen, S. Krause, *Inorg. Chem.* 20 (1981) 2750.
- [61] I.B. Bersuker, *Chem. Rev.* 101 (2001) 1067.
- [62] R.J. Deeth, L.J.A. Hearnshaw, *Dalton Trans.* (2006) 1092.
- [63] J. Villa, J. Bentzien, A. Gonzalez-Lafont, J.M. Lluch, J. Bertran, A. Warshel, *J. Comput. Chem.* 21 (2000) 607.
- [64] T.V. Albu, J.C. Corchado, D.G. Truhlar, *J. Phys. Chem. A* 105 (2001) 8465.
- [65] K.D. Nielson, A.C.T. van Duin, J. Oxgaard, W.Q. Deng, W.A. Goddard, *J. Phys. Chem. A* 109 (2005) 493.
- [66] J.S. Griffiths, *The Theory of Transition-Metal Ions*, Cambridge University Press, Cambridge, 1961.
- [67] R.J. Deeth, D.L. Foulis, B.J. Williams-Hubbard, *Dalton Trans.* (2003) 3949.
- [68] R.J. Deeth, D.L. Foulis, *Phys. Chem. Chem. Phys.* 4 (2002) 4292.
- [69] W. Kaim, B. Schwederski, *Bioinorganic Chemistry: Inorganic Elements in the Chemistry of Life*, John Wiley and Sons Ltd, Chichester, 1994.
- [70] E.I. Solomon, R.K. Szilagyi, S.D. George, L. Basumallick, *Chem. Rev.* 104 (2004) 419.
- [71] B.L. Vallee, R.J.P. Williams, *Proc. Natl. Acad. Sci. U.S.A.* 59 (1968) 498.
- [72] B.G. Malmstrom, *Eur. J. Biochem.* 223 (1994) 711.
- [73] U. Ryde, M.H.M. Olsson, K. Pierloot, B.O. Roos, *J. Mol. Biol.* 261 (1996) 586.
- [74] R.J. Deeth, *Chem. Commun.* (2006) 2551.
- [75] R.J. Deeth, *Inorg. Chem.* 46 (2007) 4492.
- [76] M.H.M. Olsson, U. Ryde, B.O. Roos, K. Pierloot, *J. Biol. Inorg. Chem.* 3 (1998) 109.
- [77] U. Ryde, M.H.M. Olsson, *Int. J. Quantum Chem.* 81 (2001) 335.
- [78] C. Diedrich, R.J. Deeth, *Inorg. Chem.* 47 (2008) 2494.
- [79] J.J. Gajewski, K.E. Gilbert, T.W. Kreek, *J. Comp. Chem.* 19 (1998) 1167.
- [80] H. Lin, D.G. Truhlar, *Theor. Chem. Acc.* 117 (2007) 185.
- [81] A. Warshel, *Annu. Rev. Biophys. Biomol. Struct.* 32 (2003) 425.
- [82] F. Jensen, P.O. Norrby, *Theor. Chem. Acc.* 109 (2003) 1.
- [83] P. Comba, M. Zimmer, *Inorg. Chem.* 33 (1994) 5368.
- [84] P. Comba, T.W. Hambley, M. Strohle, *Helv. Chim. Acta* 78 (1995) 2042.
- [85] J.P. Piquemal, B. Williams-Hubbard, N. Fey, R.J. Deeth, N. Gresh, C. Giessner-Prettre, *J. Comput. Chem.* 24 (2003) 1963.
- [86] N. Gresh, *J. Comput. Chem.* 16 (1995) 856.
- [87] S.M. Woodley, P.D. Battle, C.R.A. Catlow, J.D. Gale, *J. Phys. Chem. B* 105 (2001) 6824.
- [88] A.V. Sinitsky, M.B. Darhovskii, A.L. Tchougreeff, I.A. Misurkin, *Int. J. Quantum Chem.* 88 (2002) 370.
- [89] M.B. Darhovskii, M.G. Razumov, I.V. Pletnev, A.L. Tchougreeff, *Int. J. Quantum Chem.* 88 (2002) 588.
- [90] M.B. Darkhovskii, I.V. Pletnev, A.L. Tchougreeff, *J. Comput. Chem.* 24 (2003) 1703.
- [91] A.L. Tchougreeff, *Int. J. Quantum Chem.* 107 (2007) 2519.